

## RESEARCH ARTICLE

10.1002/2015JG003271

## Key Points:

- The terrestrial biosphere strongly influences atmospheric  $^{14}\text{C}$  over northern Wisconsin, USA
- Simulations for the 2010 growing season results in an underestimate of the biospheric  $^{14}\text{C}$  source compared to observations
- An underestimate in the magnitude of heterotrophic respiration flux in the model or short-term ecosystem variability is suspected

## Supporting Information:

- Supporting Information S1

## Correspondence to:

B. W. LaFranchi,  
bwlafra@sandia.gov

## Citation:

LaFranchi, B. W., et al. (2016), Strong regional atmospheric  $^{14}\text{C}$  signature of respired  $\text{CO}_2$  observed from a tall tower over the midwestern United States, *J. Geophys. Res. Biogeosci.*, 121, 2275–2295, doi:10.1002/2015JG003271.

Received 11 NOV 2015

Accepted 6 AUG 2016

Accepted article online 10 AUG 2016

Published online 31 AUG 2016

## Strong regional atmospheric $^{14}\text{C}$ signature of respired $\text{CO}_2$ observed from a tall tower over the midwestern United States

B. W. LaFranchi<sup>1,2</sup>, K. J. McFarlane<sup>1</sup>, J. B. Miller<sup>3,4</sup>, S. J. Lehman<sup>5</sup>, C. L. Phillips<sup>1,6</sup>, A. E. Andrews<sup>3</sup>, P. P. Tans<sup>3</sup>, H. Chen<sup>4,7</sup>, Z. Liu<sup>2,8</sup>, J. C. Turnbull<sup>4,9</sup>, X. Xu<sup>10</sup>, and T. P. Guilderson<sup>1</sup>

<sup>1</sup>Center for Accelerator Mass Spectrometry, Lawrence Livermore National Laboratory, Livermore, CA, USA, <sup>2</sup>Now at Combustion Research Facility, Sandia National Laboratories, Livermore, California, USA, <sup>3</sup>Global Monitoring Division, NOAA Earth Systems Research Laboratory, Boulder, Colorado, USA, <sup>4</sup>Cooperative Institute for Research in Environmental Sciences, University of Colorado Boulder, Boulder, Colorado, USA, <sup>5</sup>Institute for Arctic and Alpine Research, University of Colorado Boulder, Boulder, Colorado, USA, <sup>6</sup>Now at Department of Crops and Soil Science, Oregon State University, Corvallis, Oregon, USA, <sup>7</sup>Center for Isotope Research, Energy and Sustainability Research Institute Groningen, University of Groningen, Groningen, Netherlands, <sup>8</sup>Now at Ramboll Environ US Corporation, Novato, California, USA, <sup>9</sup>National Isotope Centre, GNS Science, Lower Hutt, New Zealand, <sup>10</sup>Department of Earth System Science, University of California, Irvine, California, USA

**Abstract** Radiocarbon in  $\text{CO}_2$  ( $^{14}\text{C}$ ) measurements can aid in discriminating between fast (<1 year) and slower (>5–10 years) cycling of C between the atmosphere and the terrestrial biosphere due to the  $^{14}\text{C}$  disequilibrium between atmospheric and terrestrial C. However,  $^{14}\text{C}$  in the atmosphere is typically much more strongly impacted by fossil fuel emissions of  $\text{CO}_2$ , and, thus, observations often provide little additional constraints on respiratory flux estimates at regional scales. Here we describe a data set of  $^{14}\text{C}$  observations from a tall tower in northern Wisconsin (USA) where fossil fuel influence is far enough removed that during the summer months, the biospheric component of the  $^{14}\text{C}$  budget dominates. We find that the terrestrial biosphere is responsible for a significant contribution to  $^{14}\text{C}$  that is 2–3 times higher than predicted by the Carnegie-Ames-Stanford approach terrestrial ecosystem model for observations made in 2010. This likely includes a substantial contribution from the North American boreal ecoregion, but transported biospheric emissions from outside the model domain cannot be ruled out. The  $^{14}\text{C}$  enhancement also appears somewhat decreased in observations made over subsequent years, suggesting that 2010 may be anomalous. With these caveats acknowledged, we discuss the implications of the observation/model comparison in terms of possible systematic biases in the model versus short-term anomalies in the observations. Going forward, this isotopic signal could be exploited as an important indicator to better constrain both the long-term carbon balance of terrestrial ecosystems and the short-term impact of disturbance-based loss of carbon to the atmosphere.

### 1. Introduction

Over industrialized continental regions, depletions in the ratio of radiocarbon to total carbon in atmospheric  $\text{CO}_2$  ( $^{14}\text{C}$ , expressed as  $\Delta^{14}\text{C}$ ) are driven largely by geographic gradients in fossil fuel  $\text{CO}_2$  emissions [Djuricin et al., 2012; Gamnitzer et al., 2006; Hsueh et al., 2007; Lehman et al., 2013; Levin et al., 2003, 2008, 2013; Miller et al., 2012; Randerson et al., 2002; Riley et al., 2008; Turnbull et al., 2009, 2015; Vay et al., 2009; Vogel et al., 2010, 2013]. As a consequence, a growing number of studies have used measurements of  $\Delta^{14}\text{C}$  in the troposphere to derive mole fractions of recently added fossil  $\text{CO}_2$  ( $C_{\text{ff}}$ ) while recognizing the need to correct for what are usually modest contributions to the  $^{14}\text{C}$  budget from nonfossil sources. This correction includes the respiration of  $\text{CO}_2$  from terrestrial carbon stocks containing C assimilated a decade or two ago when atmospheric  $^{14}\text{C}$  was higher (the so-called terrestrial biospheric disequilibrium isoflux).

The biospheric disequilibrium is commonly exploited in studies of ecosystem C dynamics as it can directly reveal information about the “age” of C in different soil reservoirs [Marin-Spiotta et al., 2008; McFarlane et al., 2013; Paul et al., 1997; Torn et al., 2005; Trumbore, 1993; Trumbore and Druffel, 1983]. These studies take advantage of what is known as “excess bomb radiocarbon,” which was produced in the atmosphere as a result of above ground nuclear weapons testing during the midtwentieth century and resulted in a near doubling of the atmospheric  $^{14}\text{C}$  content. When the 1963 atmospheric test ban treaty was ratified and above

ground testing ceased, the anthropogenic production of  $^{14}\text{C}$  in the atmosphere dropped dramatically (with a much smaller contribution persisting from nuclear power production), and the excess bomb radiocarbon in the atmosphere began to equilibrate with the terrestrial biosphere and ocean reservoirs. Since the late 1980s, there has been a positive disequilibrium between the Earth's biosphere and the atmosphere, in which the radiocarbon content in soils and plants is generally elevated with respect to the atmosphere [Naegler and Levin, 2009a, 2009b; Randerson et al., 2002]. This biospheric disequilibrium has been studied at soil plot scales to investigate soil C transit/turnover times [Froberg et al., 2011; Gaudinski et al., 2000; Huang et al., 2011], to discriminate between autotrophic and heterotrophic respiration of  $\text{CO}_2$  [Carbone et al., 2008; Czimczik et al., 2006; Phillips et al., 2013], and to identify the source of biomass C lost to the atmosphere during wildfires [Heckman et al., 2013; Schuur et al., 2003], as a few examples. These types of studies have shaped much of what we know about soil C dynamics. Studies of atmospheric  $\Delta^{14}\text{CO}_2$  at remote background sites [Graven et al., 2012b; Naegler and Levin, 2009b] have also revealed critical information about C cycling between the atmosphere and the terrestrial biosphere, from a global or hemispheric perspective. What are missing, however, are regional-scale ( $10^{-5}$ – $10^6 \text{ km}^2$ ) observations that can be used to bridge the spatial gaps between plot-level and global/hemispheric scales in the evaluation of terrestrial ecosystem models. Here we present a dataset that can be used for such a purpose.

One of the goals of this study is to explore the relationship between regional atmospheric  $\Delta^{14}\text{CO}_2$  and terrestrial ecosystem carbon cycling in the North American boreal forest. We begin by introducing some basic conceptual ideas and equations that describe the cycling of carbon within terrestrial ecosystems. Thompson and Randerson [1999] provide an excellent and thorough description of these concepts and equations that we summarize in the following discussion. In the simplest representation, a terrestrial ecosystem can be described as a system with a single input of C (photosynthetic uptake) and a first-order loss mechanism returning C to the atmosphere. Defining the input as net primary productivity (NPP), and ignoring disturbance-based loss mechanisms such as wildfire or drought, the mass balance equation can be expressed as

$$\frac{dC_{\text{stor}}}{dt} = F_{\text{NPP}} - F_{\text{resp}}, \quad (1)$$

where  $C_{\text{stor}}$  is the amount of C stored in the terrestrial ecosystem at any given time,  $F_{\text{NPP}}$  is the net primary productivity (NPP) flux, and  $F_{\text{resp}}$  is the heterotrophic respiration flux. Representing  $F_{\text{resp}}$  as a single first-order sink, the rate equation for  $F_{\text{resp}}$  is expressed as the product of  $C_{\text{stor}}$  and a first-order rate constant ( $k$ ), having units of inverse time:

$$F_{\text{resp}} = kC_{\text{stor}} \quad (2)$$

From this rate equation (2), the turnover time ( $\tau_o$ ) for the system can be defined as  $k^{-1}$ , or the ratio of  $C_{\text{stor}}$  to  $F_{\text{resp}}$ :

$$\tau_o = \frac{1}{k} = \frac{C_{\text{stor}}}{F_{\text{resp}}} \quad (3)$$

A related variable, transit time ( $\tau$ ), is defined as the amount of time a carbon atom spends in the terrestrial biosphere between photosynthetic uptake and respiration. The  $^{14}\text{C}$  signature of respired carbon ( $\Delta_{\text{resp}}$ ) at any given point in time ( $t$ ) depends on the distribution of  $\tau$  for the population of respired C atoms ( $F_{\text{resp}}(\tau)$ ) and the convolution of that distribution with historical atmospheric  $\Delta^{14}\text{CO}_2$  ( $\Delta_{\text{atm}}$ ), and  $\Delta_{\text{resp}}$  can be expressed through equation (4).

$$\Delta_{\text{resp}}(t) = \int F_{\text{resp}}(\tau)\Delta_{\text{atm}}(t - \tau)d\tau / \int F_{\text{resp}}(\tau)d\tau \quad (4)$$

Note that on decadal time scales the impact of radioactive decay of carbon while stored in the terrestrial ecosystem is negligible relative to variability in  $\Delta_{\text{atm}}$  during the twentieth century.

In a single box representation, the mean transit time ( $\bar{\tau}$ ) is equivalent to  $\tau_o$  but for more complicated and realistic representations with multiple interconnected reservoirs,  $\bar{\tau} = \tau_o$  only at steady state (when  $F_{\text{NPP}} = F_{\text{resp}}$ ). Nevertheless, the two values are closely associated [Thompson and Randerson, 1999] and  $\Delta_{\text{resp}}$ , therefore, contains information about  $\tau_o$  for the terrestrial ecosystem. For a single box representation the relationship between  $\Delta_{\text{resp}}$  and  $\tau_o$  is straightforward. Solving the differential equation that describes the single box system (equation (1)) with  $F_{\text{NPP}}$  set to zero and  $F_{\text{resp}} = C_{\text{stor}}/\tau_o$  (via equations (2) and (3)) results in an exponentially

decaying  $C_{\text{stor}}(\tau)$ , as described in equation (5) (ignoring the arbitrary pre-exponential term), where  $\tau$  replaces  $t$  and is referenced to the point in time when the decay starts. Substituting this equation for  $C_{\text{stor}}(\tau)$  into equation (3) then allows us to solve for  $F_{\text{resp}}(\tau)$  (equation (6)).

$$C_{\text{stor}}(\tau) = e^{-\tau/\tau_o} \quad (5)$$

$$F_{\text{resp}}(\tau) = \frac{e^{-\tau/\tau_o}}{\tau_o} \quad (6)$$

Equation (6), in combination with equation (4), then offers a simple way to understand the relationship between  $\tau_o$  and  $\Delta_{\text{resp}}$  and, by extension, the influence of  $\tau_o$  on the atmospheric  $^{14}\text{C}$  budget. As we will show, the peak in  $\Delta_{\text{atm}}$  in the early 1960s combined with the exponentially decaying transit time distribution,  $F_{\text{resp}}(\tau)$ , results in a peak in estimated  $\Delta_{\text{resp}}$ , when  $\tau_o \approx 30$  years (for C respired in 2010), which is nearly 6 times lower than the peak in  $\Delta_{\text{atm}}$ . In reality, the relationship between  $\tau_o$  and  $\Delta_{\text{resp}}$  is less clear (and not unique) for a system with multiple interconnected reservoirs, and different model frameworks result in different relationships between these two values. Nevertheless, the first-order kinetics controlling the flow of C through these more complicated systems results in a similar relationship between  $\tau_o$  and  $\Delta_{\text{resp}}$  (to that predicted by equations (4) and (6)), suggesting an upper limit to  $\Delta_{\text{resp}}$  that is much lower than the peak  $\Delta_{\text{atm}}$  and provides a general framework for trying to derive meaning about  $\tau_o$  from measurements of  $\Delta_{\text{resp}}$  or  $\Delta_{\text{atm}}$ .

Here we report atmospheric  $\Delta^{14}\text{CO}_2$  results from the LEF tall tower in northern Wisconsin (USA). Using a Lagrangian particle dispersion model (LPDM) in conjunction with  $^{14}\text{CO}_2$  and  $\text{CO}_2$  emissions data from multiple sources, we evaluate possible contributions to a seasonally elevated  $\Delta^{14}\text{CO}_2$  signal at LEF and show that the observations are substantially influenced by terrestrial ecosystem respiration from both the North American boreal ecoregion as well as the temperate forests and agricultural regions of the midwestern United States. We will show that minimal fossil fuel and nuclear emissions to the north and northwest of the site enable boreal biospheric emissions to be particularly well constrained by these observations, thus providing a unique opportunity to evaluate the regional-scale dynamics influencing  $F_{\text{resp}}$  and  $\Delta_{\text{resp}}$  over a critically important and potentially vulnerable ecosystem.

## 2. Methods

### 2.1. Observation Site

In this study we use measurements of  $\text{CO}_2$  mole fractions and  $\Delta^{14}\text{CO}_2$  from flask samples collected at the LEF tall tower, located in northern Wisconsin, USA (45.9451°N, 90.2732°W). The LEF tower is one of eight North American tall towers in the NOAA Global Monitoring Division (NOAA-GMD, hereafter) Global Greenhouse Gas Reference Network (GGGRN). The base of the tower is at 472 m above sea level, and at the top it reaches 447 m above ground. The intake inlet for all observations described in this study is at 396 m above ground. The tower has been in operation as an atmospheric observatory since 1994. LEF is surrounded by mixed temperate forest/wetland complex and relatively sparse population density. It lies within Price County which has a population density of  $\sim 5 \text{ km}^{-2}$ . The nearest town is Park Falls (population  $\sim 2500$ ), which lies 6 km to the west. The closest large population center is the Minneapolis-St. Paul metropolitan area, which lies 250 km to the southwest and has a population of about 3.3 million (U.S. Census Bureau, <http://quickfacts.census.gov/qfd/index.html>). Additionally, we use  $\Delta^{14}\text{CO}_2$  from two reference sites: Niwot Ridge, Colorado USA (NWR, 40.05°N 105.59°W, 3223 m above sea level (asl)) [Lehman et al., 2013], part of the NOAA-GMD GGGRN (<http://www.esrl.noaa.gov/gmd/ccgg>) and Barrow, Alaska USA (PTB, 71.3°N, 156.6°W, 11 m asl), part of the GGGRN sampling program, but with sample preparation and measurement occurring at University of California, Irvine (X. Xu, unpublished results, 2014). Intercomparisons between the relevant  $\Delta^{14}\text{C}$  measurement programs (including a number of additional radiocarbon laboratories) are ongoing, with initial results showing a high level of agreement between the laboratories contributing data to this study [Miller et al., 2013]. The locations of these three sites can be seen in the map in Figure 1.

### 2.2. Sampling and Measurements

A detailed description of the NOAA-GMD tall tower measurement program can be found in Andrews et al. [2014] and at <http://www.esrl.noaa.gov/gmd/ccgg/towers/>. Measurements of  $\Delta^{14}\text{CO}_2$  were included as part of the flask analysis program at LEF from 2010 to the end of 2012, and methods for this program are identical

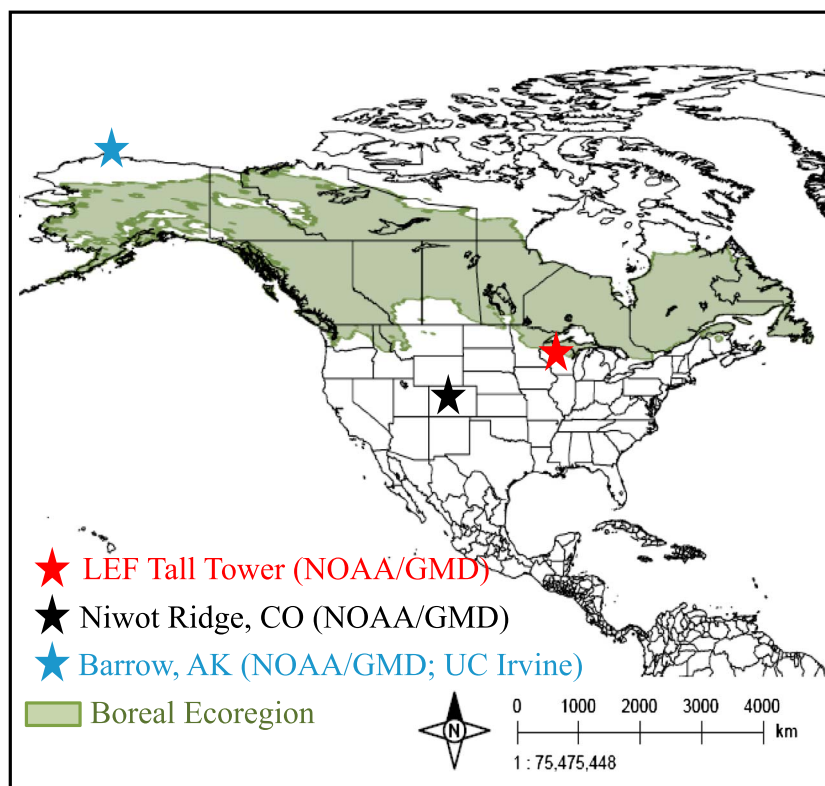


**Figure 1.** Map of North America showing three observations sites used in this study: LEF tall tower (LEF, NOAA/GMD), Niwot Ridge (NWR, NOAA/GMD), and Barrow, AK (BRW, NOAA/GMD, UC Irvine). The North American boreal ecoregion is shaded in green.

to those described in *LaFranchi et al.* [2013], including the conditional selection of air samples for analysis of  $\Delta^{14}\text{CO}_2$ . The selection was based on a visual inspection of continuous CO and  $\text{CO}_2$  data, aimed at providing a consistent mix of both anthropogenically impacted and “background” air samples. For the first  $\sim 15$  months of the study period, samples were collected for  $\Delta^{14}\text{CO}_2$  every  $\sim 3$  days and thereafter once every  $\sim 6$  days. Sampling occurred at midday (12:00–14:00 local standard time) for all samples used in this analysis. Two flasks were filled within 5 min of each other ( $\sim 4$  standard liters total) to provide enough air for analysis of  $\Delta^{14}\text{CO}_2$ , which typically requires 0.4 to 0.5 mg C for high-precision ( $< 3\%$ ) analysis, as well as the standard measurement suite of trace gases [*Andrews et al.*, 2014].

$\Delta^{14}\text{CO}_2$  was analyzed by extraction of  $\text{CO}_2$  from the whole air samples using cryogenic separation followed by reduction of extracted  $\text{CO}_2$  to graphite for atom counting via accelerator mass spectrometry (AMS). Extractions of authentic samples, measurement controls, and process blanks were performed at the University of Colorado Institute for Arctic and Alpine Research (INSTAAR) Laboratory for AMS Radiocarbon Preparation and Research (NSRL) using an automated extraction system [*Turnbull et al.*, 2010]. Graphitization and AMS analysis of the LEF samples were done at Lawrence Livermore National Laboratory's (LLNL) Center for Accelerator Mass Spectrometry (CAMS). A description of the high-precision methods for analysis of atmospheric samples at CAMS is given by *Graven et al.* [2007]. Results are expressed as age-corrected  $\Delta^{14}\text{CO}_2$  in units of per mille (‰), calculated from the measured  $^{14}\text{C}/^{13}\text{C}$  ratio, corrected for mass-dependent fractionation, measured relative to NBS Oxalic Acid I (OX1) and reported relative to the absolute radiocarbon standard, as detailed in *Stuiver and Polach* [1977] (note that in the Stuiver and Polach work,  $\Delta$  is equivalent to what we refer to as  $\Delta^{14}\text{CO}_2$ ). Because the CAMS AMS does not measure the  $^{13}\text{C}/^{12}\text{C}$  ratio online, we use  $\delta^{13}\text{C}$  values measured in the same flask samples from INSTAAR Stable Isotope Laboratory [*Vaughn et al.*, 2004] for normalization. Dry air mole fractions of  $\text{CO}_2$  were measured at NOAA-GMD on one of two nearly identical automated analytical systems. These systems consist of custom-made

gas inlet systems, calibration systems, gas-specific analyzers, and system-control software. A nondispersive infrared analyzer is used for CO<sub>2</sub> measurement with an uncertainty <0.1 ppm [Conway *et al.*, 1994].

Uncertainty in  $\Delta^{14}\text{CO}_2$  observations is determined as the standard deviation ( $1\sigma$ ) of a series of repeat measurements on extraction aliquots of whole air stored in high-pressure cylinders. Air from two surveillance cylinders with different but near-ambient  $^{14}\text{C}$  activities, identified as NWT3 and NWT4, were extracted, graphitized, and analyzed concurrently with the LEF samples across seven different measurement “wheels” or batches. Multiple samples of NBS Oxalic Acid II (“OX2,” a commonly used secondary standard) were combusted, graphitized, and analyzed simultaneously. Typically, in a wheel containing 25 authentic samples, 10 primary OX1 standards, 12 measurement controls (6 OX2, 3 NWT3, and 3 NWT4), and 1 process blank were analyzed. To date, 192 NWT3 and NWT4 samples have been measured at CAMS, including those measured with the LEF observations described in this study as well as those measured with samples from two other sites in the NOAA-GMD GGGRN. The ( $1\sigma$ ) repeatability (standard deviation) of these NWT3 and NWT4 samples was  $\pm 2.4\%$  ( $n = 192$ ), which we consider to be the single sample uncertainty in this analysis. In a small number of cases, the internal variability on the measurement of an unknown sample was larger than the repeatability of the pool of NWT3 and NWT4 control samples. For these measurements, we assign the larger uncertainty value.

### 2.3. Simulations of Atmospheric $^{14}\text{CO}_2$ : Lagrangian Atmospheric Transport Model

Two different Lagrangian particle dispersion models (LPDM), the Hybrid Single-Particle Lagrangian Integrated Trajectory (HYSPPLIT) atmospheric transport model [Draxler and Hess, 1998; Hegarty *et al.*, 2013] and the Flexible Particle (FLEXPART) model [Seibert and Frank, 2004; Stohl *et al.*, 2005], were used to trace the sampled air masses at LEF back in time in order to quantify the sensitivity of each  $\Delta^{14}\text{CO}_2$  observation to upwind surface emissions. The HYSPPLIT model was run in the STILT (Stochastic Time-Inverted Lagrangian Transport) emulation mode, in which particles were driven backward for 10 days by the 3-hourly archived meteorological winds from the North American Mesoscale Forecast System (NAM, <http://www.emc.ncep.noaa.gov/index.php?branch=NAM>) with a spatial resolution of 12 km, and the density of the particles was used to compute the influence function or “footprint” at a spatial resolution of  $1^\circ \times 1^\circ$ . The FLEXPART model simulates 10 day back trajectories of 10,000 particles released from LEF driven by wind fields simulated by WRF (v3.5.1) [Brioude *et al.*, 2013; Skamarock and Klemp, 2008]. The WRF model was run with initial and boundary conditions and 6-hourly domain-wide nudging provided by ERA-Interim reanalysis (<http://rda.ucar.edu/datasets/ds627.0/>). The WRF domain covers North America (latitude: 14.81°N–62.32°N; longitude 55.21°W–138.79°W) with 12 km horizontal resolution and has 50 layers vertically up to 10 hPa. The FLEXPART-WRF output has 12 km spatial resolution and consists of a residence time weighted by the atmospheric density in the surface layer (0–100 m above ground level), which are converted to footprints used for the  $\Delta^{14}\text{CO}_2$  simulation.

Both models result in 240-hourly footprints for each of the 114  $\Delta^{14}\text{CO}_2$  samples collected at LEF in 2010, covering the 10 days prior to the collection of each sample. The footprints carry units of [ppm/( $\mu\text{mol m}^{-2} \text{s}^{-1}$ )]. Convolution with surface flux data (in units of  $\mu\text{mol m}^{-2} \text{s}^{-1}$ ) and integrating over time and space results in a simulated mole fraction contribution (in ppm) at the air sampling location resulting from that particular emission source.

### 2.4. Simulating Atmospheric $^{14}\text{CO}_2$ Gradients ( $\delta\Delta$ )

In this analysis we compare modeled and observed spatial gradients in  $\Delta^{14}\text{CO}_2$  at the LEF tower with respect to regional background observations, annotated hereafter as  $\delta\Delta_{\text{mod}}$  and  $\delta\Delta_{\text{obs}}$ , respectively. We define  $\delta\Delta_{\text{obs}}$  as the difference in  $\Delta^{14}\text{CO}_2$  between the LEF observations ( $\Delta_{\text{LEF}}$ ) and a reference background observation ( $\Delta_{\text{bkg}}$ ) at either Niwot Ridge, CO, or Barrow, AK (equation (7)).

$$\delta\Delta_{\text{obs}} = \Delta_{\text{LEF}} - \Delta_{\text{bkg}} \quad (7)$$

The background values used in the calculation of  $\delta\Delta$  are derived from observations using the CCGCRV smoothing function [Thoning *et al.*, 1989], which removes short-term variability that may not be representative of larger-scale processes. For NWR, the smoothing function is applied to observations described in Lehman *et al.* [2013]. For BRW, the smoothing function is applied to previously unpublished observations (X. Xu, unpublished results). Sensitivity of monthly average  $\delta\Delta$  estimates to the input parameters of the smoothing function is on the order of 0.1–0.3%.

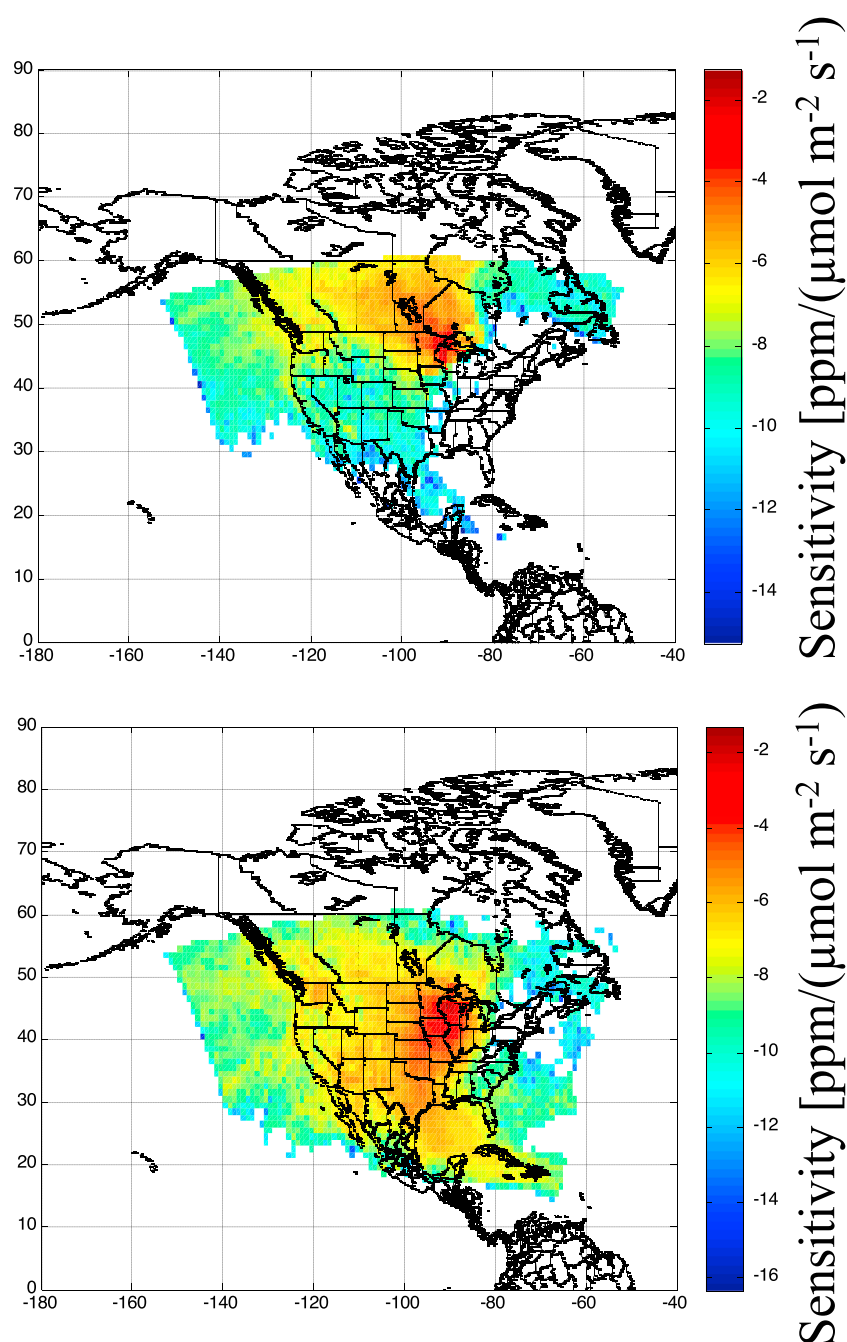


**Figure 2.** HYSPLIT footprints for LEF observations in 2010, showing average sensitivity functions for samples grouped into (a) northerly influence and (b) southerly influence. Note that color scale is logarithmic.

We use the HYSPLIT footprints to determine, on a sample-by-sample basis, which background site to apply to each sample. To do this, each analyzed air sample is categorized based on two generalized simulated transport patterns: those with predominately northern influence and those with predominately southern influence. The categorization is done through a visual inspection of each sample's time-integrated footprint. Of the 114  $\Delta^{14}\text{CO}_2$  observations during 2010, 65 show clear northern influence, 47 show clear southern influence, and 2 additional samples are not adequately represented by either category (these 2 samples are ignored in the following analysis). Using the FLEXPART footprints results in a similar distribution, with about 80% of samples being categorized identically to the categorization resulting from the HYSPLIT analysis. The average HYSPLIT footprints for the northern and southern samples are shown in Figure 2. For the northerly

**Table 1.** Description of Model Inputs Used to Estimate  $\delta\Delta$  at LEF

Variable	Inventory/Data Source (Native Grid Size)	Time Resolution	Notes
Nuclear $^{14}\text{C}$ emissions	2010 PRIS power output (IAEA) for North America	Monthly averages	<i>Graven and Gruber</i> [2011] emission ratios and uncertainty
Wildfire $\text{CO}_2$ emissions	GFED (v3.1) database ( $0.5^\circ \times 0.5^\circ$ )	Daily averages	$^{14}\text{CO}_2$ estimates from <i>Schuur et al.</i> [2003]—Alaska controlled boreal burn
Heterotrophic respiration	CASA terrestrial ecosystem model ( $1^\circ \times 1^\circ$ )	Monthly averages	Impulse response transformation, from <i>Thompson and Randerson</i> [1999]
Fossil $\text{CO}_2$	Carbon Tracker 2011 (oi) (North American $1^\circ \times 1^\circ$ zoom region)	Monthly averages	Specific for 2010; “Miller” prior flux; $\pm 20\%$ uncertainty assumed [ <i>Gurney et al.</i> , 2011]
Atmospheric transport	WRF-FLEXPART ( $0.1^\circ \times 0.1^\circ$ )	Hourly	WRF generated winds (see text for details)
Atmospheric transport	HYSPLIT ( $1^\circ \times 1^\circ$ )	Hourly	12 km meteorology from NAM-12

samples, the BRW background values are used for calculating  $\delta\Delta_{\text{obs}}$ , and for the southerly samples, the NWR background values are used.

Using this pseudo-Lagrangian approach to subtract  $\Delta_{\text{bkg}}$  allows us to focus on components of the  $^{14}\text{CO}_2$  budget that are influenced by regionally relevant fluxes, and variability in  $\Delta_{\text{LEF}}$  can be described by the following equations, adapted from *Miller et al.* [2012]:

$$\frac{dC_{\text{LEF}}}{dt} = F_{\text{ff}} + F_{\text{resp}} + F_{\text{NPP}} + F_{\text{fire}} + \frac{dC_{\text{bkg}}}{dt} \quad (8)$$

$$C_{\text{LEF}} \frac{d\Delta_{\text{LEF}}}{dt} = (\Delta_{\text{ff}} - \Delta_{\text{bkg}})F_{\text{ff}} + (\Delta_{\text{resp}} - \Delta_{\text{bkg}})F_{\text{resp}} + (\Delta_{\text{NPP}} - \Delta_{\text{bkg}})F_{\text{NPP}} + (\Delta_{\text{fire}} - \Delta_{\text{bkg}})F_{\text{fire}} + \text{iso}F_{\text{nuc}} \quad (9)$$

In these equations,  $C$  refers to  $\text{CO}_2$  mole fractions,  $\Delta$  refers to the  $^{14}\text{C}$  isotopic signature (normalized to  $^{13}\text{C}$  according to *Stuiver and Polach* [1977]) of various carbon reservoirs,  $F$  refers to fluxes of  $\text{CO}_2$  between those reservoirs and the atmosphere, and  $\text{iso}F$  refers to pure fluxes of  $^{14}\text{CO}_2$  that can affect  $\Delta_{\text{LEF}}$  but do not impact the total  $\text{CO}_2$  budget. The subscripts for each of these general terms describe the different reservoirs and flux types: “resp” = respiration; “fire” = wildfire; “ff” = fossil fuels; “NPP” = net primary productivity; “nuc” = nuclear; and “bkg” = background. Note that equation (9) excludes ocean and cosmogenic production terms, because we do not expect these to impose horizontal gradients of  $\Delta^{14}\text{CO}_2$  at the surface over the modeled domain [*Turnbull et al.*, 2009]. In equation (9), which describes the isotopic mass balance of  $^{14}\text{CO}_2$  in atmosphere, the  $\text{CO}_2$  fluxes ( $F_x$ ) are weighted by differences between the isotopic signature of the reservoir ( $\Delta_x$ ) and  $\Delta_{\text{bkg}}$ , which is significant for each reservoir in equation (8) except for NPP. Because of the fast cycling associated with NPP and because normalization to  $\delta^{13}\text{C}$  in the definition of  $\Delta$  accounts for mass-dependent fractionation [*Stuiver and Polach*, 1977],  $\Delta_{\text{NPP}}$  is effectively equivalent to  $\Delta_{\text{bkg}}$  and the NPP term in equation (8) can be ignored. The so-called biospheric disequilibrium flux, described above, is represented by the  $F_{\text{resp}}$  term in equation (8) and, unlike NPP, cannot be ignored due to the substantial fraction of respired carbon that was fixed in prior growing seasons when  $\Delta_{\text{bkg}}$  was higher. Similarly, wildfire can contribute to the isotopic mass balance of the atmosphere through the rapid release of stored carbon that is elevated in  $^{14}\text{C}$  with respect to the recent atmosphere. The “nuc” isoflux refers to anthropogenic production and subsequent release to the atmosphere of  $^{14}\text{C}$  and must be referenced as an isoflux because it cannot be directly characterized by a finite isotopic ratio.

We simulate  $\delta\Delta$  by modeling the individual components of the isotopic mass balance equation (equation (9)). For this analysis we consider  $\delta\Delta$  to be a function only of the contributions from  $F_{\text{resp}}$ ,  $F_{\text{fire}}$ ,  $F_{\text{ff}}$ , and  $\text{iso}F_{\text{nuc}}$ , for which we define individual contributing components to  $\delta\Delta_{\text{mod}}$ :

$$\delta\Delta_{\text{mod}} = \delta\Delta_{\text{ff}} + \delta\Delta_{\text{biosph}} + \delta\Delta_{\text{fire}} + \delta\Delta_{\text{nuc}} \quad (10)$$

Each component of  $\delta\Delta_{\text{mod}}$  is simulated as a convolution of the footprint surface sensitivity functions and  $\text{CO}_2$  fluxes with an assigned or calculated signature or with pure  $^{14}\text{CO}_2$  fluxes. The flux data used in this analysis are of three general types: (1) those for fossil fuel and wildfire  $\text{CO}_2$  fluxes (in  $\mu\text{mol CO}_2 \text{ m}^{-2} \text{ s}^{-1}$ ) for which a single  $\Delta$  value (with, for wildfire, prescribed uncertainty) is imposed on the emitted  $\text{CO}_2$ ; (2) isofluxes (in  $\mu\text{mol CO}_2 \text{ m}^{-2} \text{ s}^{-1} \text{ ‰}$ ) in which both the  $\text{CO}_2$  flux and the associated  $\Delta$  varies in space and time, as with the biospheric disequilibrium flux; and (3) pure  $^{14}\text{CO}_2$  fluxes for nuclear emissions (in units of  $\mu\text{mol }^{14}\text{CO}_2 \text{ m}^{-2} \text{ s}^{-1}$ )

where the total CO<sub>2</sub> emissions are negligible. Note that nuclear emissions can also be expressed as an isoflux (for consistency with equation (9)) by dividing by the <sup>14</sup>C/C ratio of the Modern Standard ( $R_s = 1.176 \times 10^{-12}$ ) and converting to ‰. Table 1 summarizes the emissions data sources used, the spatial and temporal resolution of the emissions, and the uncertainties associated with each flux estimate. After integrating the convolved footprints and emissions over space and time, the result is a CO<sub>2</sub> mole fraction excess ( $\delta C_x$ ) for fossil and wildfire emissions (type 1), a disequilibrium excess ( $\delta C_x(\Delta_x - \Delta_{\text{bkg}})$ ) for biodisequilibrium emissions (type 2), or a <sup>14</sup>CO<sub>2</sub> activity excess ( $\delta A_x$ ) for nuclear emissions (type 3), where “excess” refers to the enhancement at the site resulting from within-domain (i.e., regional scale) fluxes. These excess values are converted to  $\delta\Delta$  through equation (11) for type 1 and type 2 emissions described above and equation (12) for type 3 emissions:

$$\delta\Delta_x = \delta C_x \frac{\Delta_x - \Delta_{\text{bkg}}}{C_{\text{obs}}} \quad (11)$$

$$\delta\Delta_x = \delta A_x \frac{1000\text{‰}}{R_s C_{\text{obs}}} \quad (12)$$

In these equations,  $C_{\text{obs}}$  is the observed CO<sub>2</sub> mole fraction at LEF,  $R_s$  is the <sup>14</sup>C/C ratio of the Modern Standard (as defined above), and subscript “x” refers to each modeled component the total  $\delta\Delta$  signal (ff, fire, resp, and nuc). The derivation of  $\delta\Delta_x$  using mass balance considerations is provided in Appendix A. Equation (11) is used to calculate  $\delta\Delta$  for the fossil fuel, wildfire, and respiration sources, while equation (12) is used to calculate  $\delta\Delta_{\text{nuc}}$ . The fossil fuel term ( $\delta\Delta_{\text{ff}}$ ) is calculated using the “Miller” CarbonTracker fossil fuel emissions from CarbonTracker CT2011\_oi ([http://www.esrl.noaa.gov/gmd/ccgg/carbontracker/CT2011\\_oi/documentation\\_ff.html#ct\\_doc](http://www.esrl.noaa.gov/gmd/ccgg/carbontracker/CT2011_oi/documentation_ff.html#ct_doc)) and defining  $\Delta_{\text{ff}} = -1000\text{‰}$  for these emissions. Note that biofuels used for transportation (such as ethanol in gasoline) are not included in the fossil fuel inventory. Uncertainty for fossil fuel emissions is prescribed to be 20% for this study. According to a survey of uncertainties in the Vulcan fossil fuel emissions data product [Gurney *et al.*, 2011], the highest uncertainty for any individual county in the United States is ~20%. We expect uncertainties at the regional scale, therefore, to be lower than 20% and view this as a conservative estimate of uncertainty in  $\delta\Delta_{\text{ff}}$  for this study. Fire CO<sub>2</sub> ( $C_{\text{fire}}$ ) is calculated using emissions from the Global Fire Emissions Database (GFEDv3.1, [https://daac.ornl.gov/VEGETATION/guides/global\\_fire\\_emissions\\_v3.1.html](https://daac.ornl.gov/VEGETATION/guides/global_fire_emissions_v3.1.html)) [van der Werf *et al.*, 2006], which is a wild fire data product and does not include domestic wood burning. The estimates for  $\Delta_{\text{fire}}$  are highly uncertain and likely vary with location, among different vegetation types, and with fire intensity. Despite this, we use a single value for  $\Delta_{\text{fire}}$  that was determined from a Keeling-plot estimate downwind of a controlled boreal forest burn in Alaska (i.e., 210‰ from Schuur *et al.* [2003], but we allow for high uncertainty by taking the upper and lower estimates from a survey of different potential sources of biomass (including vegetation components and soil horizons) as uncertainty limits (350 and 110 ‰, respectively, which correspond, roughly, to mean biomass ages of 38 and 5 years [Schuur *et al.*, 2003]). Note that these values are likely biased high since the Schuur *et al.* study took place nearly 10 years prior to the present study and further equilibration between the atmosphere and other reservoirs has occurred, resulting in a decrease in the isotopic disequilibrium between the atmospheric and terrestrial biosphere. Nuclear power emissions are estimated using the same methodology and emission ratios as Graven and Gruber [2011], but updated with monthly power outputs for each North American reactor for 2010, obtained from the International Atomic Energy Association (IAEA) Power Reactor Information System (PRIS, <http://www.iaea.org/pris/>). This is a parameterized approach in which different reactor types are assigned specific <sup>14</sup>CO<sub>2</sub> emission factors. Vogel *et al.* [2013] highlight the flaws in this approach, noting that individual reactors can have strongly varying emission factors over time. To account for this, we apply large uncertainties in the emission factors (for example, ±60% for boiling water reactors and –95% to +250% for heavy water reactors) to the resultant emissions, according to Graven and Gruber [2011]. Any additional <sup>14</sup>CO<sub>2</sub> emissions during reactor maintenance will not be captured but may be sporadically significant [Vogel *et al.*, 2013]. Further, any <sup>14</sup>C emitted as <sup>14</sup>CH<sub>4</sub> and subsequently oxidized to <sup>14</sup>CO<sub>2</sub> is ignored. Although <sup>14</sup>CH<sub>4</sub> is the dominant molecular form of <sup>14</sup>C emitted from reactors in the U.S., where pressurized water reactors are the primary reactor type, due to the relatively long lifetime (~7–10 years) of CH<sub>4</sub> with respect to its oxidation to CO<sub>2</sub>, the influence of <sup>14</sup>CH<sub>4</sub> emissions on the observed  $\Delta^{14}\text{CO}_2$  gradient is likely to be negligible across our domain.

The biospheric disequilibrium analog for equation (11) is obtained through a convolution of the impulse response function [Thompson and Randerson, 1999] of the Carnegie-Ames-Stanford Approach (CASA)

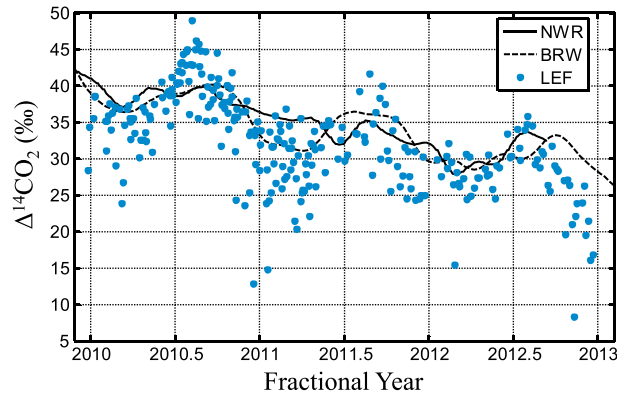


**Figure 3.** Time series of  $\Delta^{14}\text{CO}_2$  at LEF (blue circles) from 2010 to 2012, with smoothed NWR (black solid line) and BRW (black dashed line) observations shown for reference. Residuals about the smoothed curves are on the order of the single sample measurement uncertainty (approximately 2‰).

biosphere (the response). The response of the model over time provides the transit time distribution of C returning to the atmosphere via heterotrophic respiration at any given point in time, or  $F_{\text{resp}}(\tau)$ , as described above and defined in equation (6) for a single box terrestrial biosphere. Through these simulations,  $F_{\text{resp}}(\tau)$  is calculated for each  $1^\circ \times 1^\circ$  CASA grid cell and is updated monthly. The gridded simulation of  $F_{\text{resp}}(\tau)$  is transformed into a gridded biospheric disequilibrium isoflux ( $\text{iso}F_{\text{bioidis}}$ ) through equation (13), where  $t$  is the time at which  $\text{iso}F_{\text{bioidis}}$  is calculated (for each month in 2010 for this study). The convolution of the time-dependent gridded estimate of  $\text{iso}F_{\text{bioidis}}(t)$  with the observation footprints provides the simulated value  $\delta C_{\text{resp}}(\Delta_{\text{bioidis}})$  for each LEF sample, where  $\Delta_{\text{bioidis}} = \Delta_{\text{resp}} - \Delta_{\text{bkg}}$ , thus giving the disequilibrium excess ( $\delta\Delta_{\text{bioidis}}$ ), through equation (11). We initially assign uncertainty limits that are equivalent to double and 50% of the modeled  $\delta\Delta_{\text{bioidis}}$ . Later, we treat this component of the budget as an unknown variable to be evaluated through the comparison of model and observations.

$$\text{iso}F_{\text{bioidis}}(t) = \int F_{\text{resp}}(\tau)(\Delta_{\text{atm}}(t - \tau) - \Delta_{\text{atm}}(t)) d\tau \quad (13)$$

We can also calculate some diagnostics to aid in the interpretation of the simulations of  $\delta\Delta_{\text{bioidis}}$ , including  $F_{\text{resp}}$ ,  $\bar{\tau}$ ,  $\Delta_{\text{bioidis}}$ , and  $\Delta_{\text{resp}}$  through equations (14)–(16a), (16b), respectively. Note that  $C_{\text{resp}}$  can be obtained through the convolution of the gridded  $F_{\text{resp}}$  with the observational footprints, as for other components of the C budget as described above.

$$F_{\text{resp}} = \int F_{\text{resp}}(\tau) d\tau \quad (14)$$

$$\bar{\tau} = \frac{\int F_{\text{resp}}(\tau)\tau d\tau}{\int F_{\text{resp}}(\tau) d\tau} \quad (15)$$

$$\Delta_{\text{bioidis}}(t) = \frac{\int F_{\text{resp}}(\tau)(\Delta_{\text{atm}}(t - \tau) - \Delta_{\text{atm}}(t)) d\tau}{\int F_{\text{resp}}(\tau) d\tau} \quad (16a)$$

$$\Delta_{\text{resp}} = \Delta_{\text{bioidis}} + \Delta_{\text{atm}} \quad (16b)$$

### 3. Results and Discussion

#### 3.1. Observations

The time series of  $\Delta^{14}\text{CO}_2$  observed at LEF from 2010 to the end of 2012 is shown in Figure 3, along with smoothed background records from NWR [Lehman et al., 2013] and BRW (X. Xu, unpublished results, 2014), both of which are decreasing at a rate of approximately  $5\text{‰ yr}^{-1}$ . A consistent sinusoidal seasonal pattern is evident in the LEF data over all three years that has a maximum in the summer and a minimum in the winter, qualitatively similar to what has been observed elsewhere over North America [Graven et al., 2012a; LaFranchi et al., 2013; Lehman et al., 2013; Miller et al., 2012]. Determination of  $\delta\Delta_{\text{obs}}$  (equation (7)) is an

biogeochemical model [Field et al., 1995; Randerson et al., 1996; Thompson et al., 1996; Malmstrom et al., 1997] with the atmospheric  $\Delta^{14}\text{C}$  history ( $\Delta_{\text{atm}}$ ). This procedure has been used previously to estimate  $\Delta_{\text{resp}}$  as a correction to estimates of  $C_{\text{ff}}$  [Lehman et al., 2013; Miller et al., 2012; Turnbull et al., 2007] and is described in detail by Thompson and Randerson [1999]. Briefly, a discrete NPP pulse is applied to the CASA model (the impulse), after which the model is followed forward in time (for 200 years) until all but a negligible amount of C is left in the terrestrial

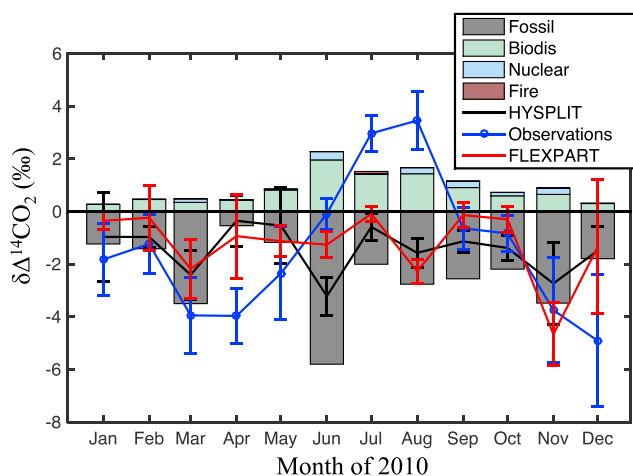


**Figure 4.** Monthly median observations of  $\delta\Delta$  (blue line) alongside the model results, including HYSPLIT simulations (black line) and FLEXPART simulations (red line) for 2010. The individual contributions to  $\delta\Delta_{\text{mod}}$  are also shown for the HYSPLIT simulations (bars), including  $\delta\Delta_{\text{resp}}$ ,  $\delta\Delta_{\text{nuc}}$ ,  $\delta\Delta_{\text{wfr}}$ , and  $\delta\Delta_{\text{ff}}$ . Error bars are standard errors for  $\delta\Delta_{\text{obs}}$  and the quadrature sum of uncertainties from each contributing emission source for  $\delta\Delta_{\text{mod}}$  (see Table 1 for details).

NWR during these months (see Figure 3). However, there is negligible dependence on the selection of background during the summertime, which is the main period of interest for this study. The summertime enhancement, with respect to the background sites, is strongest in 2010, decreasing somewhat in 2011 and 2012.

### 3.2. Simulations

Figure 4 also shows two estimates of monthly  $\delta\Delta_{\text{mod}}$ , calculated using the FLEXPART and HYSPLIT models for the 2010 samples, with broad agreement found between both model estimates. This finding is consistent with a recent study showing that three widely used LPDMs (HYSPLIT, STILT, and FLEXPART) have comparable skill in simulating the plumes from controlled tracer release experiments [Hegarty *et al.*, 2013]. Since both models used here are driven by different underlying meteorology and are calculated at different spatial resolutions, it suggests that this analysis is relatively insensitive to likely errors in the transport component of the models. Therefore, for the remainder of this analysis we will focus solely on the HYSPLIT model calculations, though our conclusions remain the same whether using HYSPLIT or FLEXPART.

Estimates of  $\delta\Delta_{\text{mod}}$  from HYSPLIT are separated into each individual budget term in Figure 4. The biospheric disequilibrium, fire, and nuclear components of the budget are positive contributions to  $\delta\Delta_{\text{mod}}$ , while the fossil component is a negative contribution. The biospheric disequilibrium is by far the largest of the three positive contributions to  $\delta\Delta_{\text{mod}}$ . The magnitude of  $\delta\Delta_{\text{biodis}}$  has a seasonal pattern that roughly coincides with the growing season, consistent with expectations of more heterotrophic respiration in the summer months. The highest simulated  $\delta\Delta_{\text{biodis}}$  occurs during June when it averages (median) 2.0‰ (1.0‰–3.9‰, based on uncertainty estimates in emissions of –50% and +100%).

The nuclear component is the next largest positive contribution. Even though the power output values that drive the emission rates have a slight seasonal dependence, with a maximum during winter, the simulated  $\delta\Delta_{\text{nuc}}$  shows little to no seasonal pattern, with variability that correlates more strongly with changes in the strength and geographic distribution of the observation footprint. The  $\delta\Delta_{\text{nuc}}$  term is generally small but increases when surface sensitivity is substantial over the midwestern United States (to the south of LEF) where there are more reactors. For samples that are appreciably impacted by nuclear emissions ( $\delta\Delta_{\text{nuc}} > 0.1\text{‰}$ ,  $n = 36$ ), the mean  $\delta\Delta_{\text{nuc}}$  is simulated to be 0.8‰ (0.3‰–1.5‰, based on emissions uncertainty) with the most strongly impacted sample having a  $\delta\Delta_{\text{nuc}}$  of 3.4‰ (1.4‰–5.8‰). Because different types of nuclear reactors have different uncertainties associated with their  $^{14}\text{CO}_2$  emission factors [Graven and Gruber, 2011], the second most strongly impacted sample actually has a higher upper uncertainty limit: 2.7‰ (0.3‰–9.1‰).

attempt to isolate the portion of the observed LEF  $\Delta^{14}\text{CO}_2$  that arises from regional and local influences. Figure 4 shows monthly  $\delta\Delta_{\text{obs}}$  for 2010, calculated using sample specific background values from either BRW or NWR (as described above).

The general pattern of  $\delta\Delta_{\text{obs}}$  shows negative values in the winter and spring (roughly between October and March) and increasingly positive values throughout the summer, with a maximum in August. Using the sample specific backgrounds results in a slightly less negative  $\Delta^{14}\text{CO}_2$  in the winter and spring than would have been estimated using the NWR backgrounds alone because of the slightly more negative  $\Delta^{14}\text{CO}_2$  at BRW than at

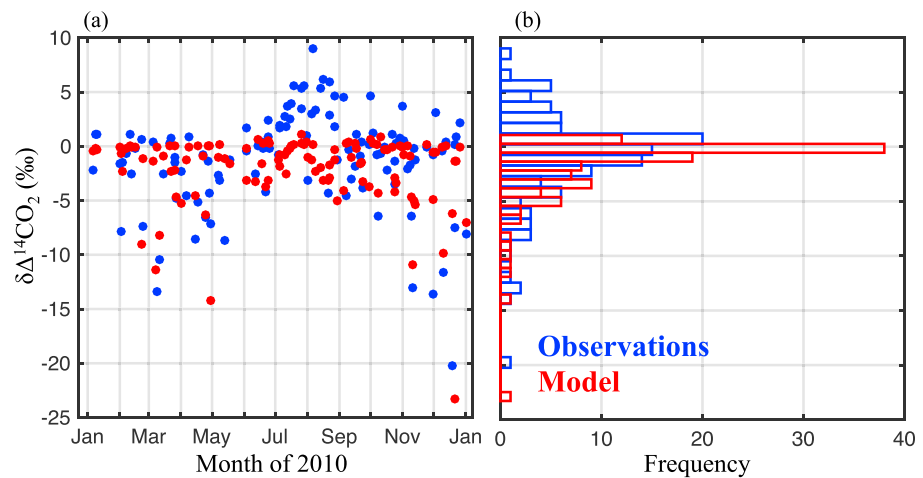


**Figure 5.** (a) Time series and (b) histogram of individual observations (blue) and simulations (red) of  $\delta\Delta$ . Model and observations are shown for 2010 only.

According to CarbonTracker 2013B (<http://www.esrl.noaa.gov/gmd/ccgg/carbontracker/fluxtimeseries.php>), which assimilates wildfire information from GFED [van der Werf *et al.*, 2006], wildfire activity was relatively high in boreal North America in 2010 compared to other recent years (second highest since 2000). Despite this, wildfire emissions account for a small fraction of the monthly  $^{14}\text{CO}_2$  budget and are detectable only in the months of June and July. In reality, the impact of this source is likely even smaller since the assumed  $^{14}\text{C}$  disequilibrium is likely an upper limit (as described above). Since wildfires tend to be discrete events in both time and space, it is not surprising that the associated signal will be small when summing across a large geographic footprint and averaging at monthly time scales. The simulations estimate 11 total samples that have meaningful influence from wildfires ( $\delta\Delta_{\text{fire}} > 0.1\text{‰}$ ). With the exception of one sample collected in November, all of the fire-influenced samples were collected between June and August. The amount of  $C_{\text{fire}}$  simulated at LEF ranges from 0.1 to 1.7 ppm for these 11 samples, with the most strongly fire-influenced sample carrying a  $\delta\Delta_{\text{fire}}$  value of 0.8‰ (0.3‰–1.4‰, uncertainty range for  $\Delta_{\text{fire}}$ ).

The fossil contributions to  $\delta\Delta_{\text{mod}}$  on a point-by-point basis exhibit a wide range of values with a median of  $-2.6\text{‰}$  and a maximum of  $-16.8\text{‰}$ . Monthly medians range from  $-0.5\text{‰}$  to  $-5.8\text{‰}$ . There is little to no apparent seasonal pattern to the modeled fossil fuel emissions signal at LEF. Across the entire year, the fossil contribution is the largest contributor to  $\delta\Delta_{\text{mod}}$  in terms of absolute magnitude in any given month, and it is dominant between November and March. As a result, the total monthly average  $\delta\Delta_{\text{mod}}$  is always negative.

### 3.3. Comparison of Simulations and Observations

The comparison of  $\delta\Delta_{\text{obs}}$  and  $\delta\Delta_{\text{mod}}$  in Figure 4 shows that there are additional positive contributions to  $\delta\Delta_{\text{obs}}$  that the model does not reproduce. Figure 5 also shows this data as both a time series (Figure 5a) and as a histogram (Figure 5b) of observed and modeled  $\delta\Delta$  for all samples. In the histogram, the observations show a distribution of values around zero that extends to positive values as high as  $+9\text{‰}$  and has a tail that extends to large negative values, indicating some strongly fossil-influenced samples. The modeled distribution, on the other hand, is strongly skewed toward negative values with a high frequency of samples around 0 and very few values significantly above zero.

The time series of  $\delta\Delta_{\text{obs}}$  shows that the frequency of observations that are greater than the  $1\sigma$  measurement precision ( $2.4\text{‰}$ ) above zero is strongly seasonal (Figure 4 and Figure 5a), with a maximum during the late summer months. The seasonal cycle of this observed enrichment is similar to that of the modeled  $\delta\Delta_{\text{biodis}}$ , although it peaks slightly later in the year (July–August) than  $\delta\Delta_{\text{biodis}}$  (June–July). The contribution of  $\delta\Delta_{\text{nuc}}$  on the other hand has a highly variable distribution across the year with no apparent seasonality. To explore the geographic distribution of this summertime enrichment, we analyze the model versus observation differences for the two geographic transport regimes shown in Figure 2. From the average of the observational footprints it can be seen that the “northerly samples” are primarily influenced by emissions over the remote

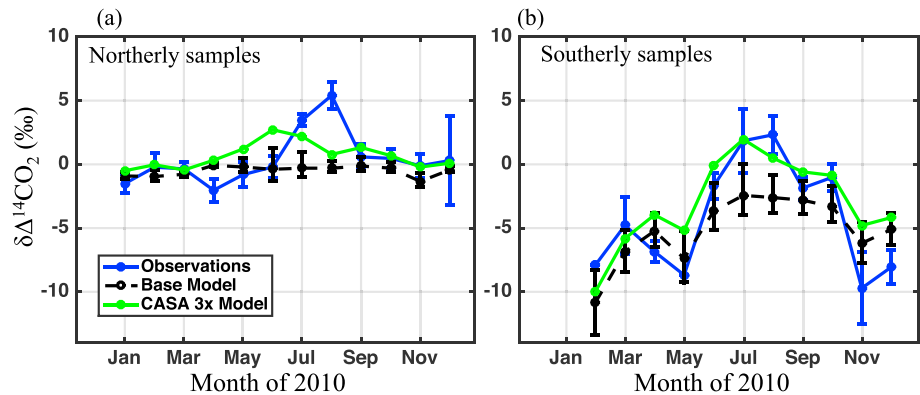


**Figure 6.** Monthly median observations (from equation (7)) (blue) and HYSPLIT simulations (black: base model; green: 3x CASA model) for the (a) northerly samples and (b) southerly samples. Error bars are standard errors for  $\delta\Delta_{bs}$  and the quadrature sum of uncertainties from each contributing emission source for  $\delta\Delta_{mod}$  (see Table 1 for details).

boreal forest of central and northwestern Canada, where there is relatively low population density and minimal fossil CO<sub>2</sub> emissions are expected. The “southerly samples,” on the other hand, are primarily influenced by emissions over the midwestern United States, where population density and fossil fuel emissions are much higher. The monthly averages of both  $\delta\Delta_{obs}$  and  $\delta\Delta_{mod}$  for the northerly and southerly samples are shown in Figures 6a and 6b, respectively. Both the model and observations exhibit higher fossil influence in the southerly samples, as indicated by the more negative  $\delta\Delta$  values on average, consistent with the spatial sensitivities delivered by the LPDMs. Although not shown here explicitly, the simulations predict significantly stronger contributions from  $\delta\Delta_{ff}$  and  $\delta\Delta_{nuc}$  in the southerly samples, significantly stronger contributions from  $\delta\Delta_{fire}$  in the northerly samples, and nearly equivalent contributions from  $\delta\Delta_{biog}$ . For both the northerly and southerly samples, the model underpredicts  $\delta\Delta_{obs}$  in the late summer months by a similar amount. The observations for both northerly and southerly samples show a strong seasonal cycle, with a minimum in the winter and spring and maximum in the late summer.

According to the model, a stronger fossil influence from the south contributes to a mean offset between the southerly samples and northerly samples of about  $-3\text{‰}$ . When viewed on a month-to-month basis (Figure 4), it appears as though the simulated seasonal cycle is damped, with too few highly depleted fossil-influenced samples during the winter and insufficiently enriched samples during the summer. When viewed on a point-by-point basis (Figure 5), however, it becomes apparent that while in the winter months the simulations do not properly reproduce the frequency and timing of the high fossil influence on the samples, they do capture the upper limit of the extent of possible fossil influence. This might be expected particularly during the winter time when mixing depths in the troposphere can be shallow and variable, thus making it more difficult to accurately simulate sensitivity to surface emissions on a consistent basis. Conversely, the underestimate of <sup>14</sup>CO<sub>2</sub> enrichment is strongest during the summer, when mixing depths are expected to be larger. The summertime underestimate is systematic, with 24 of the 50 total observations (48%) during summer (May–September) being more enriched than the maximum  $\delta\Delta_{mod}$  ( $+1.1\text{‰}$ ). For the northerly samples, exclusively, 13 samples out of 20 (or 65%) are more enriched than the maximum  $\delta\Delta_{mod}$ .

For the northerly samples, the model underestimates  $\delta\Delta_{obs}$  during midsummer, with a maximum underestimate of  $5.7\text{‰}$  ( $4.6\text{‰}$ – $6.9\text{‰}$ , the quadrature sum of uncertainties in the emission source terms and the  $1\sigma$  standard error of observations) occurring in August. On average, between May and September, the model underestimates the observations by  $2.4\text{‰}$  ( $1.5\text{‰}$ – $3.6\text{‰}$ ), with a root-mean-square deviation (RMSD) of  $3.8\text{‰}$ . For the southerly samples, the model underpredicts the observations by  $5.8\text{‰}$  ( $3.9\text{‰}$ – $8.1\text{‰}$ ) in August and by  $3.4\text{‰}$  ( $1.7\text{‰}$ – $5.6\text{‰}$ ) for May to September on average (RMSD =  $4.6\text{‰}$ ), with a seasonal cycle similar to that for the northerly samples. The larger uncertainty in the model versus observation difference for the southerly samples stems primarily from the fact that there are larger contributions from fossil sources in the southern sector. To demonstrate, the May–September average  $\delta\Delta_{ff}$  for the southern samples is  $-5.7\text{‰}$ , and the 20% uncertainty prescribed to fossil fuel emissions corresponds to  $\pm 1.1\text{‰}$  or  $\pm 32\%$  ( $1.1\text{‰}/3.4\text{‰}$ ) of the model/observation difference. In the northern samples, on the other hand, the May–September

average for  $\delta\Delta_{ff}$  is  $-1.4\text{‰}$  ( $\pm 0.3\text{‰}$ ), which translates to uncertainty in the model-observation difference of only  $\pm 13\%$ . The choice of background site applied to any given sample results in a maximum uncertainty of  $0.9\text{‰}$  (on average) during the month of May and only  $0.2\text{‰}$  for the May to September average.

### 3.4. Potential Source of “Missing” $^{14}\text{CO}_2$

The large enrichment observed makes it readily apparent that additional  $^{14}\text{CO}_2$  emissions are required to explain the observations at LEF. The missing  $^{14}\text{CO}_2$  emissions must be associated with a large and wide spread source influencing both the northerly and southerly samples and following a seasonal cycle resembling that of biospheric respiration (as represented in the underlying CASA model) with a gradual and persistent build up over the summer, rather than intermittent occurrences throughout the year. The sporadic influence of nuclear power point sources coupled with the paucity of nuclear reactors in the northern footprint makes it unlikely that the model-observation mismatch can be addressed by additional  $^{14}\text{CO}_2$  emissions from nuclear sources, even though the upper limit of uncertainty in the nuclear source is not well constrained [Vogel *et al.*, 2013]. Direct stratospheric injection of  $^{14}\text{CO}_2$  is expected to follow a different seasonal pattern than the observed excess at LEF, with peak influence occurring in spring [Appenzeller *et al.*, 1996], and is not a likely explanation. We also find no correlation between the observation/model differences in the summertime and the amount of time the sample particle back trajectories spend in the free troposphere or the average article endpoint altitude (see Figures S2 and S3). Moreover, given the fact that NWR lies at 3500 m asl (and the similarity in latitude between NWR and LEF), one might expect such a stratospheric signal to also be present, if not more significant, in the background as represented by NWR. Stratospheric influence could also, in principal, lead to a summertime anomaly in  $\delta\Delta$  through the oxidation of  $^{14}\text{CO}$  that originated in the stratosphere. While this warrants further investigation via a chemical transport model, simple back-of-the-envelope calculations making use of canonical estimates of stratosphere-troposphere exchange [Appenzeller *et al.*, 1996],  $^{14}\text{CO}$  production [Jockel *et al.*, 2002], and global OH distributions [Patra *et al.*, 2014] suggest that any locally anomalous contribution to  $\delta\Delta$  at LEF is unlikely to exceed  $1\text{‰}$ . Substantially enhanced local  $^{14}\text{CO}$  oxidation and minimal cross-latitude transport could, in theory, offset some portion of the enhancement but is not likely to fully explain the observed model-observation differences.

Emissions of  $C_{\text{fire}}$  are strongly seasonal and might conceivably contribute to the anomalous signal. However, the model results suggest that the impact of  $C_{\text{fire}}$  on our observations is small, even for summertime samples with northerly footprints, where the majority (9 out of 11 significantly impacted samples) of wildfire emissions originate. A significantly larger impact would require that the GFED database either greatly underrepresents  $\text{CO}_2$  emissions per unit area burned, greatly underdetects wildfire counts and area burned from satellite observations, or (most unlikely) that we have significantly underestimated the biodisequilibrium of burned biomass (based on Schuur *et al.* [2003]). Alternatively, postfire enhancements in  $\text{CO}_2$  respiration may be a contributing factor that would not be captured in either the GFED inventory or the CASA model in this analysis. Cumulative postfire emissions have been suggested to be just as significant as direct fire emissions [Amiro *et al.*, 2001] but spread over many years. Nonetheless, even a doubling of  $F_{\text{fire}}$  or a doubling of the isotopic disequilibrium, would have little impact on the results simulated here. Thus, the most plausible remaining explanation for the summer enrichment of  $^{14}\text{CO}_2$  observed at LEF, but not captured in the simulations, is a larger biospheric respiration  $^{14}\text{CO}_2$  source than originally calculated using CASA and the  $\Delta_{\text{atm}}$  history.

If we assume that all of the missing  $^{14}\text{CO}_2$  derives from the biospheric disequilibrium flux within the model domain,  $^{14}\text{CO}_2$  emissions estimated from the CASA impulse response functions (convolved with the atmospheric  $^{14}\text{CO}_2$  history) would need to be, on average, 3 times larger than initially specified in the model for months May through September. After considering various geographically weighted scaling functions, including a uniform scaling of the only the boreal ecoregion and a Gaussian weighting function centered at  $55^\circ\text{N}$  as suggested by Keppel-Aleks *et al.* [2012], we find that scaling the biospheric disequilibrium term uniformly throughout the North American domain by a factor of 3 results in the best agreement between model and observations (on average between May and September) (Figure 6). While the timing of the model summertime enhancement in the northerly samples is different from that of the observations, the average  $\delta\Delta_{\text{obs}}$  and  $\delta\Delta_{\text{mod}}$  between May and September agrees to be within 11% after scaling (RMSD =  $3.0\text{‰}$ ). The remaining differences (after scaling) at monthly time scales suggest that  $F_{\text{resp}}$  is delayed with respect to the base model, which is qualitatively consistent with recent findings that increased early growing season net uptake

over the north American boreal region improves agreement between CASA simulations and CO<sub>2</sub> column observations at the nearby Park Falls Total Column Carbon Observing Network (TCCON) site [Keppel-Aleks *et al.*, 2012; Messerschmidt *et al.*, 2013].

For the southern samples, the model and observations are more closely matched in phase and the average between May and September agrees to within 16% (RMSD = 3.0‰). Inclusion of an anomalous stratospheric contribution to the underestimated <sup>14</sup>CO<sub>2</sub> (using our maximum estimate of 1‰  $\delta\Delta$  in late summer) would reduce the required CASA scaling from a factor of 3 to a factor of 2.5. Our estimates of missing <sup>14</sup>CO<sub>2</sub> might also be biased if our background sites do not adequately characterize the real isotopic signature of air entering the model domain, typically at the northern or western boundaries. Given that absolute  $\Delta^{14}\text{CO}_2$  values at LEF are greater in late summer than at either NWR (latitude: 40.1°N) or BRW (latitude: 71.3°N) (Figure 3) and that atmospheric transport is dominated by mean westerly flow, it seems likely that any excess <sup>14</sup>CO<sub>2</sub> coming from outside the model domain was sourced from boreal Eurasia. Additionally, sample back trajectories exiting the northern model boundary (62°N) might also be biased as the BRW background site lies north of the model domain, although we find no correlation between the trajectory endpoint latitude and the model-observation difference (see Figure S1). Four samples have back trajectories that end south of 30°N, all of which are significantly elevated with respect to the model (see Figure S1). This may point toward an underrepresentation of  $\Delta_{\text{bkg}}$  for trajectories following trajectories far to the south. Excluding these four samples from the analysis results in a slightly lower May–September average difference between model and observations: 2.7‰ instead of 3.4‰. This results in slightly lower CASA scaling required for the southern samples as compared to the northern samples. Additional undetected boundary condition bias may exist; however, it could just as likely be in the opposite direction, thus biasing our estimate of the missing source of <sup>14</sup>CO<sub>2</sub> too low, for example, if the high-altitude NWR site is more strongly influenced by stratospheric intrusion than LEF.

According to the calculated HYSPLIT footprints, 90% of the estimated surface sensitivity for the northerly samples falls within boreal north America (cf. Figures 1 and 2a). Since the biosphere is the dominant contributor to the  $\delta\Delta$  budget in this region, it is possible to use these samples as a case study for understanding the implications of the model/observation differences for carbon ecosystem dynamics, with the understanding that the required adjustments to CASA <sup>14</sup>CO<sub>2</sub> emissions may represent an upper limit, given uncertainties in boundary conditions. Although we focus the remainder of the discussion on the boreal ecoregion, it should be noted that the applied adjustments to CASA in the temperate ecosystems to the south also appear to improve the fit of  $\delta\Delta_{\text{mod}}$  and the observations for the southerly samples.

#### 4. Implications for Terrestrial Carbon Cycling

Our ad hoc scaling of biospheric disequilibrium emissions, through equation (11), can be interpreted as either (a) an increase in the atmospheric CO<sub>2</sub> mole fraction related to (heterotrophic) respiration emissions,  $C_{\text{resp}}$  and therefore in the respiration flux ( $F_{\text{resp}}$ ); and/or (b) an increase in the isotopic signature of respiration,  $\Delta_{\text{resp}}$ , and, thereby, in  $\Delta_{\text{biadis}}$ . In the first case, the implication is that CASA simply underestimates  $F_{\text{resp}}$  and therefore the amount of respired carbon observed at LEF. The second case would suggest that the modeled (CASA)  $F_{\text{resp}}(\tau)$  within the North American boreal zone does not overlap sufficiently in time with the period of greatest  $\Delta_{\text{atm}}$  related to unassimilated excess bomb <sup>14</sup>C.

The CASA impulse response function for boreal North America (defined as the TRANSCOM region of the same name [Gurney *et al.*, 2002]) is shown in Figure 7 and is characterized by large fluxes associated with transit times less than 5 years and a long tail marked by decreasing fluxes extending out to transit times greater than 100 years. For the CASA impulse response function, we calculate  $\bar{\tau} = 30$  years (through equation (15)), corresponding to a  $\Delta_{\text{resp}}$  (equation (16b)) of 126‰ (or  $\Delta_{\text{biadis}} = 86\%$ , equation (16a)). This value represents a spatiotemporal average of transit time distributions ( $F_{\text{resp}}(\tau)$ ) across all grid cells within boreal North America. There have been recent suggestions that terrestrial ecosystem models systematically underestimate  $\tau_o$  [Carvalhais *et al.*, 2014; Koven *et al.*, 2013; Phillips *et al.*, 2015] and, consequently, the amount of stored carbon,  $C_{\text{stor}}$ . Of particular relevance is the large (~2–4 times) underestimate of  $\tau_o$  and  $C_{\text{stor}}$  in parts of boreal Canada and much of the western half of the United States [Carvalhais *et al.*, 2014], regions with substantial weighting in the LEF footprints (Figure 2). In the Carvalhais study, boreal forests were found, globally, to have

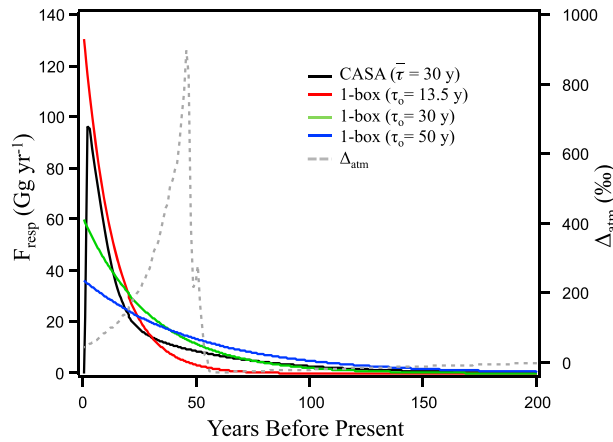


**Figure 7.** Transit time distributions of simulated ecosystem respiration for (1) boreal North America determined from the CASA impulse response function (black) and for (2) theoretical single box terrestrial ecosystems calculated using equation (7) for turnover times of 13.5 years (red), 30 years (green), and 50 year (blue). Also shown is the historical Northern Hemisphere atmospheric  $\Delta^{14}\text{CO}_2$  ( $\Delta_{\text{atm}}$ ) (adapted from *Hua et al.* [2013]) (grey dashed line).

scenarios, 13.5 years, 30 years, and 50 years (Figure 7). The integrated  $F_{\text{resp}}$  is equivalent in each case and matches that for the CASA impulse response function ( $\sim 3.6$  Pg C). The 13.5 year one-box impulse response gives an approximately equivalent  $\Delta_{\text{biodis}}$  to the CASA impulse response function (85‰).  $\Delta_{\text{biodis}}$  increases to 119‰ for  $\tau_0 = 30$  years, as more bomb carbon is incorporated into the  $F_{\text{resp}}(\tau)$  distribution. With further increases in  $\tau_0$ , however, there is increasing influence from the prebomb atmosphere, resulting in a decrease in  $\Delta_{\text{biodis}}$  for  $\tau_0 = 50$  years ( $\Delta_{\text{biodis}} = 103\%$ ) and implying an approximate upper limit to  $\Delta_{\text{biodis}}$  of around 120‰. To further illustrate this, Figure 8 shows the dependence of  $\Delta_{\text{biodis}}$  on  $\tau_0$  across a range of values from 5 years to 100 years.

These one-box scenarios suggest that there is likely to be a relatively low upper limit to  $\Delta_{\text{biodis}}$  (relative to the peak of the bomb spike) that is constrained by the long tail of  $F_{\text{resp}}(\tau)$  in the CASA impulse response and the fact that the bomb peak is relatively short lived. The changes to  $\tau_0$  in the one-box scenarios are, of course, not a perfect proxy for adjustments to  $\tau_0$  in CASA, and the shape of the  $F_{\text{resp}}(\tau)$  distribution is clearly important, as illustrated by the equivalent  $\Delta_{\text{biodis}}$  produced by both the 13.5 year one-box distribution and the 30 year

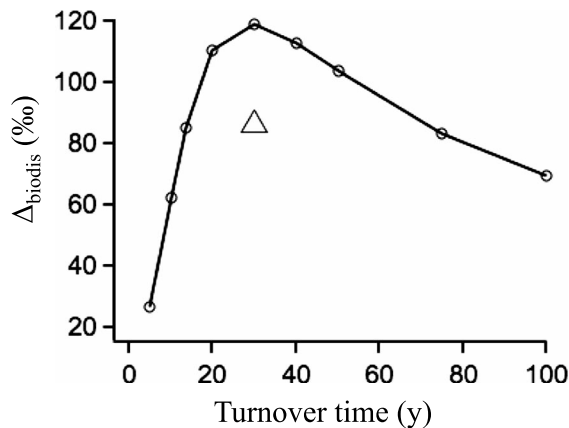


**Figure 8.**  $\Delta_{\text{biodis}}$ , calculated in 2010, as a function of turnover time ( $\tau_0$ ) for a one-box (single reservoir) terrestrial ecosystem. For comparison, the CASA  $\Delta_{\text{biodis}}$  (average over the North American boreal) is shown (triangle) at its corresponding  $\bar{\tau}$  (30 years).

$\tau_0 = 53$  years compared to previous work [Thompson and Randerson, 1999] that provided an estimate of 38 years from an impulse response transformation of boreal forests within CASA. Recall here that for CASA,  $\bar{\tau}$  does not necessarily equal  $\tau_0$  but is closely related.

Due to the nonlinearity of  $F_{\text{resp}}(\tau)$  and  $\Delta_{\text{atm}}$  over time, the response of  $\Delta_{\text{resp}}$  to an adjustment in  $\tau_0$  within CASA is not unique. However, the relationship between  $\tau_0$  and  $\Delta_{\text{resp}}$  can be approximated using a simple one-box model, for which the impulse response function can be derived analytically (Eq. (6)). We calculate transit time distributions for the one-box model using three different  $\tau_0$  ( $= \bar{\tau}$ )

CASA distribution. The long tail of the CASA distribution (see Figure 7) is responsible for the lower  $\Delta_{\text{biodis}}$  than the corresponding 30 year one-box distribution. Despite this, even for  $F_{\text{resp}}(\tau)$  derived from a combination of exponentials, the general relationship between  $\tau_0$  and  $\Delta_{\text{biodis}}$  will be consistent. Therefore, unless some mechanism is enhanced within or added to the system that significantly deemphasizes the short ( $<10$  years) and long ( $>60$  years) transit times in favor of transit times between 20 and 50 years, we are lead to conclude that an ad hoc adjustment to  $\tau_0$  within CASA is not likely to provide a

factor of 3 increase in modeled  $\delta\Delta_{\text{bioidis}}$  seemingly required to reproduce the observations at LEF. At the upper limit for  $\Delta_{\text{bioidis}}$  based on the one-box model ( $\sim 120\%$ ), the required scaling for  $F_{\text{resp}}$  reduces to a factor of 2, however.

Thus, a large change in modeled  $\delta\Delta_{\text{bioidis}}$  is more plausibly leveraged by increased  $F_{\text{resp}}$ . Moreover, there is an additional constraint that  $F_{\text{resp}}$ , which is linked to  $\tau_o$  and  $C_{\text{stor}}$  through equation (3), must be increased through an increase in  $C_{\text{stor}}$ , rather than a decrease in  $\tau_o$ . As shown in Figure 8, a decrease in  $\tau_o$  is likely to significantly decrease  $\Delta_{\text{bioidis}}$ , thereby minimizing the impact of increased  $F_{\text{resp}}$  on  $\delta\Delta_{\text{bioidis}}$  in the absence of increased terrestrial C storage. The need for increased  $C_{\text{stor}}$  is also consistent with growing evidence suggesting that  $\tau_o$  is likely significantly higher than that predicted by terrestrial ecosystem models including CASA, especially within the boreal ecoregion [Carvalhais *et al.*, 2014; Koven *et al.*, 2013]. Underlying this conclusion is the implication that in order to maintain long-term mass balance, an increase in long-term NPP or a negative  $dC_{\text{stor}}/dt$  (suggesting net C loss from the terrestrial ecosystem) would be required to accommodate the need for simultaneously higher  $F_{\text{resp}}$ ,  $C_{\text{stor}}$ , and  $\tau_o$ . Of course, mass balance within the terrestrial ecosystem is not required on a year-by-year basis, although it is consistent with the apparent need for increased  $C_{\text{stor}}$  in terrestrial ecosystem models [Carvalhais *et al.*, 2014].

As a point of reference for these findings, we can rely on a recent study using  $^{14}\text{CO}_2$  measurements to observe heterotrophic respiration directly from soils within a temperate forest close to the LEF tower [Phillips *et al.*, 2015]. The Phillips study found that  $\Delta_{\text{bioidis}}$  of respiration from a trenched soil plot was 52% on average over the growing season, which was higher than the CASA prediction (36%) for the site by about 40%. At the same time, the magnitude of  $F_{\text{resp}}$  from the same plot showed good agreement the CASA predicted heterotrophic respiration and seasonal cycle. Thus, scaling up the  $\Delta_{\text{bioidis}}$  and  $F_{\text{resp}}$  from this study would result in an increase in  $\delta\Delta_{\text{bioidis}}$  by a factor of 1.4 compared to the base CASA scenario, representing only a small improvement over the CASA predictions for the LEF observations. Note, however, that the upper limit to  $\Delta_{\text{bioidis}}$  predicted from the series of one-box models (Figure 8) applies to the entire northern hemisphere, which has seen approximately the same historical  $\Delta_{\text{atm}}$ . The CASA prediction at this temperate mid-latitude forest, therefore, could theoretically accommodate a factor of  $\sim 3$  increase in  $\Delta_{\text{bioidis}}$ , in contrast to the prediction for the boreal ecoregion which, at 86%, is much closer to the ceiling of 120%. Thus, an error in the latitudinal gradient of  $\Delta_{\text{bioidis}}$ , as estimated from the CASA impulse response functions, could theoretically impact our interpretation that a geographically uniform increase in  $F_{\text{resp}}$  is required to match the simulations to the observations at LEF. Analyzing this problem within a more sophisticated inverse modeling framework could reveal more detailed information about the temporal and spatial adjustments to  $^{14}\text{CO}_2$  emissions required for optimal agreement with the observations. In any case, the comparison with the Phillips study suggests that heterogeneity across the LEF tower footprint is significant, highlighting the importance of regional-scale observations that can be linked to gross (in addition to net) biospheric  $\text{CO}_2$  fluxes and offering motivation for repeating the Phillips study at other sites within the LEF footprint, particularly further north at a representative site within the boreal ecoregion.

A further implication of the relatively low upper limit to  $\Delta_{\text{bioidis}}$  and the associated constraint on  $F_{\text{resp}}$  over the boreal ecoregion is that NPP over the 2010 growing season can be estimated by jointly considering atmospheric  $\text{CO}_2$  and  $^{14}\text{CO}_2$  mass balance. Observations of  $\text{CO}_2$  at the LEF tower, and at the nearby TCCON site, have been used previously to constrain net ecosystem exchange (NEE) over a regional footprint [Bakwin *et al.*, 2004; Keppel-Aleks *et al.*, 2012; Messerschmidt *et al.*, 2013], including by assimilation within CarbonTracker [Peters *et al.*, 2007], which uses CASA biospheric fluxes as a prior. The optimization of NEE by these methods has resulted in the finding that increased net uptake over the boreal ecoregion, especially early in the growing season, is required to match observations of  $\text{CO}_2$ , resulting in a  $\sim 40\%$  increase in NEE (increased net uptake) over the entire growing season [Keppel-Aleks *et al.*, 2012; Messerschmidt *et al.*, 2013]. By also considering  $^{14}\text{CO}_2$  observations, it is possible for the first time to improve constraints on gross biospheric fluxes at the regional scale.

The factor of 2–3 increase in  $F_{\text{resp}}$  required to satisfy the  $^{14}\text{CO}_2$  budget in combination with prior studies finding that a factor of 1.4 increase in net uptake (as NEE) is required suggests that NPP must also increase substantially.  $C_{\text{NPP}}$  is not modeled directly in our analysis, but it can be estimated in concert with various estimates of  $C_{\text{respr}}$  given the fixed constraint on NEE set by the  $\text{CO}_2$  observations (using equation (A1) along with

modeled estimates of  $C_{ff}$  and  $C_{fire}$ ). We find that for a factor of 2–3 increase in  $C_{resp}$  (within the constraint that  $\Delta_{biodis}$  is between 86 and 120‰) relative to the base CASA scenario,  $C_{NPP}$  (and therefore the NPP flux) must increase by a factor of 1.5–2, on average, between May and September.

It is important to emphasize that this single-year study cannot necessarily point to a systematic under representation of  $F_{resp}$  and, thus, NPP, within CASA. A relevant question, therefore, is whether 2010 is an anomalous year and represents an extreme in the expected year-to-year variability in the biospheric disequilibrium emissions or whether it is more typical. Indeed, looking at the observations for 2011 and 2012 (Figure 3), it appears as though the summer enhancement at LEF decreases each year, relative to background, and CASA may better represent this part of the  $^{14}CO_2$  budget for those years. Determination of whether there are real systematic biases in CASA would require, at the very least, repeating our 2010 analysis for both 2011 and 2012, since there is likely annual variability in northerly versus southerly transport patterns and other budget terms. Further, recent findings [Parazoo *et al.*, 2015; Wolf *et al.*, 2016] that drought may have resulted in decreased  $F_{resp}$  over the midwestern and southwestern United States during 2011 and 2012 would also need to be evaluated.

It should also be noted that the impulse response transformations of terrestrial ecosystem models tend to break down outside of steady state conditions [Thompson and Randerson, 1999], so short-term (<10 years) variability, due to disturbances such as the massive insect infestation affecting western North American forests [Kurz *et al.*, 2008] or the drought impacting the United States [Parazoo *et al.*, 2015; Wolf *et al.*, 2016], is not captured by this method of estimating  $\delta\Delta_{biodis}$ . Terrestrial ecosystem disturbance would influence not only the magnitude of  $F_{resp}$  but could conceivably lead to appreciable skewing of the transit time distribution, potentially enhancing emissions of C having  $\tau$  in the range of 20–50 years. A multiyear analysis of this system, therefore, would provide valuable constraints on the terrestrial ecosystem at steady state as well as any short-term variability in  $F_{resp}$  that could also be important for constraining the long-term carbon balance.

## 5. Conclusions

We have shown that the LEF observations cannot be reproduced by model simulations, with underestimated biospheric  $^{14}CO_2$  emissions to be the likely cause. Even before accounting for the missing biospheric source of  $^{14}CO_2$ , these emissions are important contributors to the summertime  $\delta\Delta$  budget at LEF when air masses originate from both the north and the south. While the CASA terrestrial ecosystem model correctly simulates the timing of these emissions for the southerly samples, the seasonal cycle for the northerly samples and, importantly, the magnitudes for both sets of samples are poorly modeled. However, we acknowledge that limitations in our observations of the inflow conditions at the model boundary limit our ability to attribute the missing  $^{14}CO_2$  entirely to an error specifically within the model domain (and not in the background inflow). The ability to further geographically isolate this anomalous source would be of great interest, providing a regional-scale observational constraint on heterotrophic respiration, representing a critical bridge in spatial scales between those associated with plot-level and canopy-scale studies [Schuur and Trumbore, 2006] and global inversions [Naegler and Levin, 2009b]. The sensitivity of the observations to emissions from the North American boreal forest would be of particular importance, due to its large, globally significant C stores and its anticipated vulnerability to climate change.

We find that  $\delta\Delta_{biodis}$  does not further constrain  $\tau_o$  for the influencing terrestrial ecosystem due to the lack of independent constraints on  $F_{resp}$ . Nevertheless, given link between  $F_{resp}$ ,  $\tau_o$ , and  $C_{stor}$ , the observations described here can be an important barometer for terrestrial carbon cycling. Thus, the observations provide valuable information to evaluate terrestrial ecosystem models, alongside soil and vegetation stock inventories [Carvalhais *et al.*, 2014; Lichstein *et al.*, 2014; Todd-Brown *et al.*, 2013], soil carbon turnover time and  $^{14}C$  abundance [Braakhekke *et al.*, 2014; Koven *et al.*, 2013], and other parameters. A longer-term analysis of this system, enabled by more widespread  $\Delta^{14}CO_2$  observations, could lead to better understanding of biosphere-atmosphere exchange of carbon, its apparent year to year variability, and how it is impacted by large-scale climate-related disturbances such as insect epidemics, drought, fire, and permafrost melt.

## Appendix A

The following details the derivation of equations (11) and (12) in the manuscript from mass balance considerations for total C and for  $^{14}\text{C}$ (A).

$$C_{\text{obs}} = C_{\text{resp}} + C_{\text{NPP}} + C_{\text{ff}} + C_{\text{fire}} + C_{\text{bkg}} \quad (\text{A1})$$

$$A_{\text{obs}} = A_{\text{resp}} + A_{\text{NPP}} + A_{\text{ff}} + A_{\text{fire}} + A_{\text{nuc}} + A_{\text{bkg}} \quad (\text{A2})$$

Using the definition of  $\Delta$  (for simplicity, neglecting the  $^{13}\text{C}$  normalization and the factor of 1000 required for ‰ units) gives

$$\Delta_x = \frac{A_x}{C_x} - 1 \quad (\text{A3})$$

$$A_x = (\Delta_x + 1)R_s C_x \quad (\text{A4})$$

Now using the definition of equation (A4) to introduce  $\Delta$  into equation (A2) gives equation (A5).

$$(\Delta_{\text{obs}} + 1)R_s C_{\text{obs}} = (\Delta_{\text{resp}} + 1)R_s C_{\text{resp}} + (\Delta_{\text{NPP}} + 1)R_s C_{\text{NPP}} + (\Delta_{\text{ff}} + 1)R_s C_{\text{ff}} + (\Delta_{\text{fire}} + 1)R_s C_{\text{fire}} + A_{\text{nuc}} + (\Delta_{\text{bkg}} + 1)R_s C_{\text{bkg}} \quad (\text{A5})$$

Dividing through by  $R_s$  gives equation (A6), which rearranges to equation (A7):

$$(\Delta_{\text{obs}} + 1)C_{\text{obs}} = (\Delta_{\text{resp}} + 1)C_{\text{resp}} + (\Delta_{\text{NPP}} + 1)C_{\text{NPP}} + (\Delta_{\text{ff}} + 1)C_{\text{ff}} + (\Delta_{\text{fire}} + 1)C_{\text{fire}} + A_{\text{nuc}}/R_s + (\Delta_{\text{bkg}} + 1)C_{\text{bkg}} \quad (\text{A6})$$

$$\Delta_{\text{obs}}C_{\text{obs}} + C_{\text{obs}} = \Delta_{\text{resp}}C_{\text{resp}} + C_{\text{resp}} + \Delta_{\text{NPP}}C_{\text{NPP}} + C_{\text{NPP}} + \Delta_{\text{ff}}C_{\text{ff}} + C_{\text{ff}} + \Delta_{\text{fire}}C_{\text{fire}} + C_{\text{fire}} + A_{\text{nuc}}/R_s + \Delta_{\text{bkg}}C_{\text{bkg}} + C_{\text{bkg}} \quad (\text{A7})$$

Subtracting equation (A1) gives equation (A8)

$$\Delta_{\text{obs}}C_{\text{obs}} = \Delta_{\text{resp}}C_{\text{resp}} + \Delta_{\text{NPP}}C_{\text{NPP}} + \Delta_{\text{ff}}C_{\text{ff}} + \Delta_{\text{fire}}C_{\text{fire}} + A_{\text{nuc}}/R_s + \Delta_{\text{bkg}}C_{\text{bkg}} \quad (\text{A8})$$

(Note that this has the same form as *Turnbull et al.* [2009], “equation 0,” with the exception of fire and nuclear terms.)

Rearranging equation (A8) gives equation (A9):

$$\Delta_{\text{obs}}C_{\text{obs}} - \Delta_{\text{bkg}}C_{\text{bkg}} = \Delta_{\text{resp}}C_{\text{resp}} + \Delta_{\text{photo}}C_{\text{photo}} + \Delta_{\text{ff}}C_{\text{ff}} + \Delta_{\text{fire}}C_{\text{fire}} + A_{\text{nuc}}/R_s \quad (\text{A9})$$

Substituting in equation (A1) for  $C_{\text{bkg}}$  gives equation (A10):

$$\Delta_{\text{obs}}C_{\text{obs}} - \Delta_{\text{bkg}}(C_{\text{obs}} - C_{\text{resp}} - C_{\text{NPP}} - C_{\text{ff}} - C_{\text{fire}}) = \Delta_{\text{resp}}C_{\text{resp}} + \Delta_{\text{NPP}}C_{\text{NPP}} + \Delta_{\text{ff}}C_{\text{ff}} + \Delta_{\text{fire}}C_{\text{fire}} + A_{\text{nuc}}/R_s \quad (\text{A10})$$

Dividing through by  $C_{\text{obs}}$  and rearranging gives equation (A11):

$$\Delta_{\text{obs}} - \Delta_{\text{bkg}} = [\Delta_{\text{resp}}C_{\text{resp}} + \Delta_{\text{NPP}}C_{\text{NPP}} + \Delta_{\text{ff}}C_{\text{ff}} + \Delta_{\text{fire}}C_{\text{fire}} + A_{\text{nuc}}/R_s - \Delta_{\text{bkg}}(C_{\text{resp}} + C_{\text{NPP}} + C_{\text{ff}} + C_{\text{fire}})]/C_{\text{obs}} \quad (\text{A11})$$

Combining terms on the right hand side and using the fact that  $\Delta_{\text{NPP}} = \Delta_{\text{bkg}}$  gives equation (A12):

$$\Delta_{\text{obs}} - \Delta_{\text{bkg}} = [(\Delta_{\text{resp}} - \Delta_{\text{bkg}})C_{\text{resp}} + (\Delta_{\text{ff}} - \Delta_{\text{bkg}})C_{\text{ff}} + (\Delta_{\text{fire}} - \Delta_{\text{bkg}})C_{\text{fire}} + A_{\text{nuc}}/R_s]/C_{\text{obs}} \quad (\text{A12})$$

Equation (A12) can then be rewritten as

$$\Delta_{\text{obs}} - \Delta_{\text{bkg}} = \delta\Delta = \delta\Delta_{\text{resp}} + \delta\Delta_{\text{ff}} + \delta\Delta_{\text{fire}} + \delta\Delta_{\text{nuc}} \quad (\text{A13})$$

where

$$\delta\Delta_{\text{resp}} = C_{\text{resp}}(\Delta_{\text{resp}} - \Delta_{\text{bkg}})/C_{\text{obs}} \quad (\text{A14a})$$

$$\delta\Delta_{\text{ff}} = C_{\text{ff}}(\Delta_{\text{ff}} - \Delta_{\text{bkg}})/C_{\text{obs}} \quad (\text{A14b})$$

$$\delta\Delta_{\text{fire}} = C_{\text{fire}}(\Delta_{\text{fire}} - \Delta_{\text{bkg}})/C_{\text{obs}} \quad (\text{A14c})$$

$$\delta\Delta_{\text{nuc}} = A_{\text{nuc}}/(R_s C_{\text{obs}}) \quad (\text{A14d})$$

### Acknowledgments

The LEF tower data used in this study can be found at <http://www.esrl.noaa.gov/gmd/dv/iadv/>. This work was performed under the auspices of the United States Department of Energy by Lawrence Livermore National Laboratory under contract DE-AC52-07NA27344, with support from Lawrence Livermore National Laboratory (LDRD 11-ERD-053) and US DOE Office of Science (DOE-OS-OBERTES project SCW1447). Measurements at LEF and NWR are supported in part by the NOAA ESRL Global Monitoring Division with additional assistance from the NOAA Climate Program Office's Atmospheric Chemistry, Carbon Cycle and Climate program. Z.L. was supported under the Laboratory Directed Research and Development program at Sandia National Laboratories. Sandia is a multiprogram laboratory operated by Sandia Corporation, a Lockheed Martin Company, for the United States Department of Energy's National Nuclear Security Administration under contract DEAC04-94AL85000. We thank the Sandia High Performance Computing Program for their support in running FLEXPART-WRF. Assistance in radiocarbon sample preparation was provided by Paula Zermeno (CAMS), Shane Bradshaw (CAMS), Caroline Stitt (CAMS), Chad Wolak (INSTAAR), Patrick Cappa (INSTAAR), and Stephen Morgan (INSTAAR). The authors would also like to acknowledge Heather Graven for her useful suggestions during the preparation of this manuscript. We thank both anonymous reviewers for their very constructive criticism and feedback on our manuscript. Data are available at <http://www.esrl.noaa.gov/gmd/dv/iadv/>.

### References

- Amiro, B. D., B. J. Stocks, M. E. Alexander, M. D. Flannigan, and B. M. Wotton (2001), Fire, climate change, carbon and fuel management in the Canadian boreal forest, *Int. J. Wildland Fire*, *10*, 405–413, doi:10.1071/Wf01038.
- Andrews, A. E., et al. (2014), CO<sub>2</sub>, CO, and CH<sub>4</sub> measurements from tall towers in the NOAA Earth System Research Laboratory's Global Greenhouse Gas Reference Network: Instrumentation, uncertainty analysis, and recommendations for future high-accuracy greenhouse gas monitoring efforts, *Atmos. Meas. Tech.*, *7*(2), 647–687.
- Appenzeller, C., J. R. Holton, and K. H. Rosenlof (1996), Seasonal variation of mass transport across the tropopause, *J. Geophys. Res.*, *101*, 15,071–15,078, doi:10.1029/96JD00821.
- Bakwin, P. S., K. J. Davis, C. Yi, S. C. Wofsy, J. W. Munger, L. Haszpra, and Z. Barcza (2004), Regional carbon dioxide fluxes from mixing ratio data, *Tellus, Ser. B*, *56*(4), 301–311, doi:10.1111/j.1600-0889.2004.00111.x.
- Braakhekke, M. C., C. Beer, M. Schrupf, A. Ekici, B. Ahrens, M. R. Hoosbeek, B. Kruijt, P. Kabat, and M. Reichstein (2014), The use of radiocarbon to constrain current and future soil organic matter turnover and transport in a temperate forest, *J. Geophys. Res. Biogeosci.*, *119*, 372–391, doi:10.1002/2013JG002420.
- Brioude, J., et al. (2013), The Lagrangian particle dispersion model FLEXPART-WRF version 3.1, *Geosci. Model Dev.*, *6*(6), 1889–1904, doi:10.5194/gmd-6-1889-2013.
- Carbone, M. S., G. C. Winston, and S. E. Trumbore (2008), Soil respiration in perennial grass and shrub ecosystems: Linking environmental controls with plant and microbial sources on seasonal and diel timescales, *J. Geophys. Res.*, *113*, G02022, doi:10.1029/2007JG000611.
- Carvalho, N., et al. (2014), Global covariation of carbon turnover times with climate in terrestrial ecosystems, *Nature*, *514*(7521), 213, doi:10.1038/nature13731.
- Conway, T. J., P. P. Tans, L. S. Waterman, and K. W. Thoning (1994), Evidence for interannual variability of the carbon-cycle from the National-Oceanic-and-Atmospheric-Administration Climate-Monitoring-and-Diagnostics-Laboratory Global-Air-Sampling-Network, *J. Geophys. Res.*, *99*, 22,831–22,855, doi:10.1029/94JD01951.
- Czimczik, C. I., S. E. Trumbore, M. S. Carbone, and G. C. Winston (2006), Changing sources of soil respiration with time since fire in a boreal forest, *Global Change Biol.*, *12*(6), 957–971, doi:10.1111/j.1365-2486.2006.01107.x.
- Djuricin, S., X. M. Xu, and D. E. Pataki (2012), The radiocarbon composition of tree rings as a tracer of local fossil fuel emissions in the Los Angeles basin: 1980–2008, *J. Geophys. Res.*, *117*, D12302, doi:10.1029/2011JD017284.
- Draxler, R. R., and G. D. Hess (1998), An overview of the HYSPLIT<sub>4</sub> modelling system for trajectories, dispersion and deposition, *Aust. Meteorol. Mag.*, *47*(4), 295–308.
- Field, C. B., J. T. Randerson, and C. M. Malmstrom (1995), Global Net Primary Production - Combining Ecology and Remote-Sensing, *Remote Sens. Environ.*, *51*(1), 74–88, doi:10.1016/0034-4257(94)00066-V.
- Froberg, M., E. Tipping, J. Stendahl, N. Clarke, and C. Bryant (2011), Mean residence time of O horizon carbon along a climatic gradient in Scandinavia estimated by <sup>14</sup>C measurements of archived soils, *Biogeochemistry*, *104*(1–3), 227–236, doi:10.1007/s10533-010-9497-3.
- Gammitzer, U., U. Karstens, B. Kromer, R. E. M. Neubert, H. A. J. Meijer, H. Schroeder, and I. Levin (2006), Carbon monoxide: A quantitative tracer for fossil fuel CO<sub>2</sub>?, *J. Geophys. Res.*, *111*, D22302, doi:10.1029/2005JD006966.
- Gaudinski, J. B., S. E. Trumbore, E. A. Davidson, and S. H. Zheng (2000), Soil carbon cycling in a temperate forest: Radiocarbon-based estimates of residence times, sequestration rates and partitioning of fluxes, *Biogeochemistry*, *51*(1), 33–69, doi:10.1023/A:1006301010014.
- Graven, H. D., and N. Gruber (2011), Continental-scale enrichment of atmospheric <sup>14</sup>C from the nuclear power industry: Potential impact on the estimation of fossil fuel-derived CO<sub>2</sub>, *Atmos. Chem. Phys.*, *11*(23), 12,339–12,349, doi:10.5194/acp-11-12339-2011.
- Graven, H. D., T. P. Guilderson, and R. F. Keeling (2007), Methods for high-precision <sup>14</sup>C AMS measurement of atmospheric CO<sub>2</sub> at LLNL, *Radiocarbon*, *49*(2), 349–356.
- Graven, H. D., T. P. Guilderson, and R. F. Keeling (2012a), Observations of radiocarbon in CO<sub>2</sub> at La Jolla, California, USA 1992–2007: Analysis of the long-term trend, *J. Geophys. Res.*, *117*, D02302, doi:10.1029/2011JD016533.
- Graven, H. D., T. P. Guilderson, and R. F. Keeling (2012b), Observations of radiocarbon in CO<sub>2</sub> at seven global sampling sites in the Scripps flask network: Analysis of spatial gradients and seasonal cycles, *J. Geophys. Res.*, *117*, D02303, doi:10.1029/2011JD016535.
- Gurney, K. R., et al. (2002), Towards robust regional estimates of CO<sub>2</sub> sources and sinks using atmospheric transport models, *Nature*, *415*(6872), 626–630.
- Gurney, K. R., V. Chandrasekaran, D. L. Mendoza, and S. Geethakumar (2011), Quantification of uncertainty associated with NACP high resolution fossil fuel CO<sub>2</sub> emissions: updates, challenges and future plans, paper presented at North American Carbon Program All-Investigators Meeting, New Orleans, La.
- Heckman, K., J. Campbell, H. Powers, B. Law, and C. Swanston (2013), The influence of fire on the radiocarbon signature and character of soil organic matter in the Siskiyou National Forest, Oregon, USA, *Fire Ecol.*, *9*(2), 40–56, doi:10.4996/fireecology.0902040.
- Hegarty, J., R. R. Draxler, A. F. Stein, J. Brioude, M. Mountain, J. Eluszkiewicz, T. Nehrkorn, F. Ngan, and A. Andrews (2013), Evaluation of Lagrangian particle dispersion models with measurements from controlled tracer releases, *J. Appl. Meteorol. Climatol.*, *52*(12), 2623–2637, doi:10.1175/jamc-d-13-0125.1.
- Hsueh, D. Y., N. Y. Krakauer, J. T. Randerson, X. M. Xu, S. E. Trumbore, and J. R. Southon (2007), Regional patterns of radiocarbon and fossil fuel-derived CO<sub>2</sub> in surface air across North America, *Geophys. Res. Lett.*, *34*, L02816, doi:10.1029/2006GL027032.
- Hua, Q., M. Barbetti, and A. Z. Rakowski (2013), Atmospheric radiocarbon for the period 1950–2010, *Radiocarbon*, *55*(4), 2059–2072.
- Huang, Z. Q., M. R. Davis, L. M. Condon, and P. W. Clinton (2011), Soil carbon pools, plant biomarkers and mean carbon residence time after afforestation of grassland with three tree species, *Soil Biol. Biochem.*, *43*(6), 1341–1349, doi:10.1016/j.soilbio.2011.03.008.
- Jockel, P., C. A. M. Brenninkmeijer, M. G. Lawrence, A. B. M. Jeuken, and P. F. J. van Velthoven (2002), Evaluation of stratosphere-troposphere exchange and the hydroxyl radical distribution in three-dimensional global atmospheric models using observations of cosmogenic <sup>14</sup>C, *J. Geophys. Res.*, *107*(D20), 4446, doi:10.1029/2001JD001324.
- Keppel-Aleks, G., et al. (2012), The imprint of surface fluxes and transport on variations in total column carbon dioxide, *Biogeosciences*, *9*(3), 875–891, doi:10.5194/bg-9-875-2012.
- Koven, C. D., W. J. Riley, Z. M. Subin, J. Y. Tang, M. S. Torn, W. D. Collins, G. B. Bonan, D. M. Lawrence, and S. C. Swenson (2013), The effect of vertically resolved soil biogeochemistry and alternate soil C and N models on C dynamics of CLM4, *Biogeosciences*, *10*(11), 7109–7131, doi:10.5194/bg-10-7109-2013.
- Kurz, W. A., C. C. Dymond, G. Stinson, G. J. Rampley, E. T. Neilson, A. L. Carroll, T. Ebata, and L. Safranyik (2008), Mountain pine beetle and forest carbon feedback to climate change, *Nature*, *452*(7190), 987–990, doi:10.1038/nature06777.
- LaFranchi, B. W., et al. (2013), Constraints on emissions of carbon monoxide, methane, and a suite of hydrocarbons in the Colorado Front Range using observations of <sup>14</sup>C, *Atmos. Chem. Phys.*, *13*(21), 11,101–11,120, doi:10.5194/acp-13-11101-2013.

- Lehman, S. J., et al. (2013), Allocation of terrestrial carbon sources using  $^{14}\text{C}$  CO<sub>2</sub>: Methods, measurement, and modeling, *Radiocarbon*, *55*(2–3), 1484–1495.
- Levin, I., B. Kromer, M. Schmidt, and H. Sartorius (2003), A novel approach for independent budgeting of fossil fuel CO<sub>2</sub> over Europe by  $^{14}\text{C}$  CO<sub>2</sub> observations, *Geophys. Res. Lett.*, *30*(23), 2194, doi:10.1029/2003GL018477.
- Levin, I., S. Hammer, B. Kromer, and F. Meinhardt (2008), Radiocarbon observations in atmospheric CO<sub>2</sub>: Determining fossil fuel CO<sub>2</sub> over Europe using Jungfraujoch observations as background, *Sci. Total Environ.*, *391*(2–3), 211–216.
- Levin, I., B. Kromer, and S. Hammer (2013), Atmospheric Delta (CO<sub>2</sub>)-C-14 trend in Western European background air from 2000 to 2012, *Tellus, Ser. B*, *65*, 20092, doi:10.3402/tellusb.v65i0.20092.
- Lichstein, J. W., N. Z. Golaz, S. Malyshev, E. Shevliakova, T. Zhang, J. Sheffield, R. A. Birdsey, J. L. Sarmiento, and S. W. Pacala (2014), Confronting terrestrial biosphere models with forest inventory data, *Ecol. Appl.*, *24*(4), 699–715.
- Malmstrom, C. M., M. V. Thompson, G. P. Juday, S. O. Los, J. T. Randerson, and C. B. Field (1997), Interannual variation in global-scale net primary production: Testing model estimates, *Global Biogeochem. Cycles*, *11*(3), 367–392, doi:10.1029/97GB01419.
- Marin-Spiotta, E., C. W. Swanston, M. S. Torn, W. L. Silver, and S. D. Burton (2008), Chemical and mineral control of soil carbon turnover in abandoned tropical pastures, *Geoderma*, *143*(1–2), 49–62, doi:10.1016/j.geoderma.2007.10.001.
- McFarlane, K. J., M. S. Torn, P. J. Hanson, R. C. Porras, C. W. Swanston, M. A. Callahan, and T. P. Guilderson (2013), Comparison of soil organic matter dynamics at five temperate deciduous forests with physical fractionation and radiocarbon measurements, *Biogeochemistry*, *112*(1–3), 457–476, doi:10.1007/s10533-012-9740-1.
- Messerschmidt, J., N. Parazoo, D. Wunch, N. M. Deutscher, C. Roehl, T. Warneke, and P. O. Wennberg (2013), Evaluation of seasonal atmosphere-biosphere exchange estimations with TCCON measurements, *Atmos. Chem. Phys.*, *13*(10), 5103–5115, doi:10.5194/acp-13-5103-2013.
- Miller, J. B., et al. (2012), Linking emissions of fossil fuel CO<sub>2</sub> and other anthropogenic trace gases using atmospheric  $^{14}\text{C}$  CO<sub>2</sub>, *J. Geophys. Res.*, *117*, D08302, doi:10.1029/2011JD017048.
- Miller, J. B., et al. (2013), Initial results of an intercomparison of AMS-based atmospheric  $^{14}\text{C}$  CO<sub>2</sub> measurements, *Radiocarbon*, *55*(2–3), 1475–1483.
- Naegler, T., and I. Levin (2009a), Biosphere-atmosphere gross carbon exchange flux and the  $\delta^{13}\text{C}$  CO<sub>2</sub> and  $\Delta^{14}\text{C}$  CO<sub>2</sub> disequilibria constrained by the biospheric excess radiocarbon inventory, *J. Geophys. Res.*, *114*, D17303, doi:10.1029/2008JD011116.
- Naegler, T., and I. Levin (2009b), Observation-based global biospheric excess radiocarbon inventory 1963–2005, *J. Geophys. Res.*, *114*, D17302, doi:10.1029/2008JD011100.
- Parazoo, N. C., E. Barnes, J. Worden, A. B. Harper, K. B. Bowman, C. Frankenberg, S. Wolf, M. Litvak, and T. F. Keenan (2015), Influence of ENSO and the NAO on terrestrial carbon uptake in the Texas-northern Mexico region, *Global Biogeochem. Cycles*, *29*, 1247–1265, doi:10.1002/2015GB005125.
- Patra, P. K., et al. (2014), Observational evidence for interhemispheric hydroxyl-radical parity, *Nature*, *513*(7517), 219, doi:10.1038/nature13721.
- Paul, E. A., R. F. Follett, S. W. Leavitt, A. Halvorson, G. A. Peterson, and D. J. Lyon (1997), Radiocarbon dating for determination of soil organic matter pool sizes and dynamics, *Soil Sci. Soc. Am. J.*, *61*(4), 1058–1067.
- Peters, W., et al. (2007), An atmospheric perspective on North American carbon dioxide exchange: CarbonTracker, *Proc. Natl. Acad. Sci. U.S.A.*, *104*(48), 18,925–18,930, doi:10.1073/pnas.0708986104.
- Phillips, C. L., K. J. McFarlane, D. Risk, and A. R. Desai (2013), Biological and physical influences on soil  $^{14}\text{C}$  CO<sub>2</sub> seasonal dynamics in a temperate hardwood forest, *Biogeosciences*, *10*(12), 7999–8012, doi:10.5194/bg-10-7999-2013.
- Phillips, C. L., K. J. McFarlane, B. LaFranchi, A. R. Desai, J. B. Miller, and S. J. Lehman (2015), Observations of  $^{14}\text{C}$  CO<sub>2</sub> in ecosystem respiration from a temperate deciduous forest in Northern Wisconsin, *J. Geophys. Res. Biogeosci.*, *120*, 600–616, doi:10.1002/2014JG002808.
- Randerson, J. T., M. V. Thompson, C. M. Malmstrom, C. B. Field, and I. Y. Fung (1996), Substrate limitations for heterotrophs: Implications for models that estimate the seasonal cycle of atmospheric CO<sub>2</sub>, *Global Biogeochem. Cycles*, *10*(4), 585–602, doi:10.1029/96GB01981.
- Randerson, J. T., I. G. Enting, E. A. G. Schuur, K. Caldeira, and I. Y. Fung (2002), Seasonal and latitudinal variability of troposphere  $\Delta^{14}\text{C}$  CO<sub>2</sub>: Post bomb contributions from fossil fuels, oceans, the stratosphere, and the terrestrial biosphere, *Global Biogeochem. Cycles*, *16*(4), 1112, doi:10.1029/2002GB001876.
- Riley, W. J., D. Y. Hsueh, J. T. Randerson, M. L. Fischer, J. G. Hatch, D. E. Pataki, W. Wang, and M. L. Goulden (2008), Where do fossil fuel carbon dioxide emissions from California go? An analysis based on radiocarbon observations and an atmospheric transport model, *J. Geophys. Res.*, *113*, G04002, doi:10.1029/2007JG000625.
- Schuur, E. A. G., and S. E. Trumbore (2006), Partitioning sources of soil respiration in boreal black spruce forest using radiocarbon, *Global Change Biol.*, *12*(2), 165–176, doi:10.1111/j.1365-2486.2005.01066.x.
- Schuur, E. A. G., S. E. Trumbore, M. C. Mack, and J. W. Harden (2003), Isotopic composition of carbon dioxide from a boreal forest fire: Inferring carbon loss from measurements and modeling, *Global Biogeochem. Cycles*, *17*(1), 1001, doi:10.1029/2001GB001840.
- Seibert, P., and A. Frank (2004), Source-receptor matrix calculation with a Lagrangian particle dispersion model in backward mode, *Atmos. Chem. Phys.*, *4*, 51–63.
- Skamarock, W. C., and J. B. Klemp (2008), A time-split nonhydrostatic atmospheric model for weather research and forecasting applications, *J. Comput. Phys.*, *227*(7), 3465–3485, doi:10.1016/j.jcp.2007.01.037.
- Stohl, A., C. Forster, A. Frank, P. Seibert, and G. Wotawa (2005), Technical note: The Lagrangian particle dispersion model FLEXPART version 6.2, *Atmos. Chem. Phys.*, *5*, 2461–2474.
- Stuiver, M., and H. A. Polach (1977), Reporting of C-14 data—Discussion, *Radiocarbon*, *19*(3), 355–363.
- Thompson, M. V., J. T. Randerson, C. M. Malmstrom, and C. B. Field (1996), Change in net primary production and heterotrophic respiration: How much is necessary to sustain the terrestrial carbon sink?, *Global Biogeochem. Cycles*, *10*(4), 711–726, doi:10.1029/96GB01667.
- Thompson, M. V., and J. T. Randerson (1999), Impulse response functions of terrestrial carbon cycle models: Method and application, *Global Change Biol.*, *5*(4), 371–394.
- Thoning, K. W., P. P. Tans, and W. D. Komhyr (1989), Atmospheric carbon-dioxide at Mauna Loa Observatory. 2. Analysis of the NOAA GMCC data, 1974–1985, *J. Geophys. Res.*, *94*, 8549–8565, doi:10.1029/JD094iD06p08549.
- Todd-Brown, K. E. O., J. T. Randerson, W. M. Post, F. M. Hoffman, E. A. G. Schuur, and S. D. Allison (2013), Causes of variation in soil carbon simulations from CMIP5 Earth system models and comparison with observations, *Biogeosciences*, *10*(3), 1717–1736, doi:10.5194/bg-10-1717-2013.
- Torn, M. S., P. M. Vitousek, and S. E. Trumbore (2005), The influence of nutrient availability on soil organic matter turnover estimated by incubations and radiocarbon modeling, *Ecosystems*, *8*(4), 352–372, doi:10.1007/s10021-004-0259-8.
- Trumbore, S. E. (1993), Comparison of carbon dynamics in tropical and temperate soils using radiocarbon measurements, *Global Biogeochem. Cycles*, *7*, 275–290, doi:10.1029/93GB00468.

- Trumbore, S. E., and E. R. M. Druffel (1983), Carbon isotopes for characterizing sources and turnover of nonliving organic matter, in *The Role of Nonliving Organic Matter in the Earth's Carbon Cycle*, pp. 7–22, John Wiley, Chichester, U. K.
- Turnbull, J. C., S. J. Lehman, J. B. Miller, R. J. Sparks, J. R. Southon, and P. P. Tans (2007), A new high precision  $^{14}\text{C}$  time series for North American continental air, *J. Geophys. Res.*, *112*, D11310, doi:10.1029/2006JD008184.
- Turnbull, J. C., P. Rayner, J. B. Miller, T. Naegler, P. Ciais, and A. Cozic (2009), On the use of  $^{14}\text{C}$  as a tracer for fossil fuel  $\text{CO}_2$ : Quantifying uncertainties using an atmospheric transport model, *J. Geophys. Res.*, *114*, D22302, doi:10.1029/2009JD012308.
- Turnbull, J. C., S. J. Lehman, S. Morgan, and C. Wolak (2010), A new automated extraction system for  $^{14}\text{C}$  measurement for atmospheric  $\text{CO}_2$ , *Radiocarbon*, *52*(3), 1261–1269.
- Turnbull, J. C., et al. (2015), Toward quantification and source sector identification of fossil fuel  $\text{CO}_2$  emissions from an urban area: Results from the INFLUX experiment, *J. Geophys. Res. Atmos.*, *120*, 292–312, doi:10.1002/2014JD022555.
- van der Werf, G. R., J. T. Randerson, L. Giglio, G. J. Collatz, P. S. Kasibhatla, and A. F. Arellano (2006), Interannual variability in global biomass burning emissions from 1997 to 2004, *Atmos. Chem. Phys.*, *6*, 3423–3441.
- Vaughn, B. H., J. B. Miller, D. F. Ferretti, and J. C. White (2004), Stable isotope measurements of atmospheric  $\text{CO}_2$  and  $\text{CH}_4$ , in *Handbook of Stable Isotope Analytical Techniques*, edited by P. de Groot, pp. 272–304, Elsevier, San Diego, Calif.
- Vay, S. A., S. C. Tyler, Y. Choi, D. R. Blake, N. J. Blake, G. W. Sachse, G. S. Diskin, and H. B. Singh (2009), Sources and transport of delta  $^{14}\text{C}$  in  $\text{CO}_2$  within the Mexico City Basin and vicinity, *Atmos. Chem. Phys.*, *9*(14), 4973–4985.
- Vogel, F. R., S. Hammer, A. Steinhof, B. Kromer, and I. Levin (2010), Implication of weekly and diurnal  $^{14}\text{C}$  calibration on hourly estimates of  $\text{CO}_2$ -based fossil fuel  $\text{CO}_2$  at a moderately polluted site in southwestern Germany, *Tellus, Ser. B*, *62*(5), 512–520, doi:10.1111/j.1600-0889.2010.00477.x.
- Vogel, F. R., I. Levin, and D. E. J. Worthy (2013), Implications for deriving regional fossil fuel  $\text{CO}_2$  estimates from atmospheric observations in a hot spot of nuclear power plant  $^{14}\text{C}$  emissions, *Radiocarbon*, *55*(2–3), 1556–1572.
- Wolf, S., et al. (2016), Warm spring reduced carbon cycle impact of the 2012 US summer drought, *Proc. Natl. Acad. Sci. U.S.A.*, *113*(21), 5880–5885, doi:10.1073/pnas.1519620113.